Long-term serial passaging of SARS-CoV-2 reveals signatures of convergent evolution

Charles S.P. Foster[1,2,*], Gregory J. Walker[1,2], Tyra Jean[1,2], Maureen Wong[1], Levent Brassil[3], Sonia R. Isaacs[1] , Yonghui Lyu[1] , Stuart Turville[4,5], Anthony Kelleher[4,5,6,] and William D. Rawlinson[1,2,3]

[1]Serology and Virology Division (SAViD), NSW Health Pathology, Prince of Wales Hospital, Sydney, NSW 2031, Australia

[2]School of Biomedical Sciences, Faculty of Medicine & Health, University of New South Wales, Sydney, NSW 2052, Australia

[3]School of Biotechnology and Biomolecular Sciences, Faculty of Science, University of New South Wales, Sydney, NSW 2052, Australia

[4]Kirby Institute, University of New South Wales, Sydney, NSW, Australia

[5]RNA Institute, University of New South Wales, Sydney, NSW, Australia

[6]St Vincent's Hospital, Sydney, New South Wales, Australia

[*]Correspondence: charles.foster@unsw.edu.au

Abstract

Understanding viral evolutionary dynamics is crucial to pandemic responses, informing prediction of virus adaptation over time, virus adaptation to antiviral and immune pressures, design of effective therapies, and virus surveillance for public health strategies. Whole-genome sequencing (WGS) of SARS-CoV-2 has enabled fine-grained studies of virus evolution in the human population. Serial passaging *in vitro* offers a complementary controlled environment to investigate the emergence and persistence of genetic variants that may confer selective advantage. In this study, nine virus lineages, including four "variants of concern" and three former "variants under investigation", were sampled over ≥33 serial passages (range 33-100) in Vero E6 cells. WGS was used to examine virus evolutionary dynamics and identify key mutations with implications for fitness and/or transmissibility. Mutations accumulated regularly during serial passaging. Many low-frequency variants were lost but others became fixed, suggesting either *in vitro* benefits, or at least a lack of deleterious effect. Mutations arose convergently both across passage lines and compared with contemporaneous SARS-CoV-2 clinical sequences, including some hypothesised to drive lineage success through host immune evasion (e.g. S:A67V, S:H655Y). The appearance of these mutations *in vitro* suggested key mutations can arise convergently even in the absence of a multicellular host immune response through mechanisms other than immune-driven mutation. Such mutations may provide other benefits to the viruses *in vitro*, or arise stochastically. Our quantitative investigation into SARS-CoV-2 evolutionary dynamics spans the greatest number of serial passages to date, and will inform measures to reduce the effects of SARS-CoV-2 infection on the human population.

Importance

The ongoing evolution of SARS-CoV-2 has challenged public health efforts to minimise the health impacts of the virus during the COVID-19 pandemic. Carrying out whole-genome sequencing of outbreak cases has enabled global contact tracing efforts and the identification of mutations of concern within the virus' genome. Here, we use a complementary approach of charting the evolution of the virus within a controlled cell culture environment, focusing on nine different virus lineages. Our approach demonstrates how SARS-CoV-2 continues to evolve readily in vitro, with many changes mirroring those seen in outbreak cases globally. Findings of the study are important for investigating how important mutations arise, and considering the future evolutionary trajectory of SARS-CoV-2.

Introduction

The COVID-19 pandemic saw whole-genome sequencing (WGS) embraced on an unprecedented scale, with nearly 100 countries worldwide possessing SARS-CoV-2 WGS capability and contributing to publicly available sequencing repositories (Chen et al., 2022). Consequently, the number of high quality full-genome sequences for SARS-CoV-2 (>15,000,000 as of January 2025) far exceeds that of any other pathogen. The availability of these sequencing data have allowed the population-scale evolution of SARS-CoV-2 to be characterised with fine-grained detail, facilitating real-time monitoring of the spread of SARS-CoV-2, identification of new viral lineages, and have provided crucial insights into virus evolution. For example, the rise and fall of different SARS-CoV-2 lineages has been charted, with attempts to link the presence of key mutations with lineage success in spreading through the human population. This wealth of genomic data has been vital in guiding public health responses, vaccine design, and antiviral treatments (Markov et al., 2023).

Global sequencing efforts have revealed that SARS-CoV-2 has continued to accumulate mutations throughout its genome since first emerging globally in 2020. The rate of mutation accumulation within SARS-CoV-2 (~1×10^{-6} to 2×10^{-6} mutations per nucleotide per replication cycle) is typical of betacoronaviruses, but below the rate typical in other RNA viruses that lack proofreading mechanisms (Markov et al., 2023). Charting the changes accruing in the SARS-CoV-2 genome in real time has allowed quantitative inference of evolutionary processes, such as the diversification of the virus into distinct phenotypes with different transmissibility, disease severity, and immune evasion properties (Markov et al., 2023). Retrospective consideration can divide the COVID-19 pandemic into several 'eras': the initial phase of the pandemic characterised by apparently limited evolution of the virus, the sudden emergence of the highly divergent virus lineages with altered phenotypes (variants of concern, VOCs) (Tay et al., 2022), and periods of gradual evolution within VOC lineages (Lythgoe et al., 2023; Tay et al., 2022). Determining the evolutionary forces responsible for each of these eras is key to understanding how the pandemic has progressed over time, how it will continue to progress as SARS-CoV-2 shifts towards being an endemic virus (Lavine et al., 2021), and how future pandemics might unfold.

Analysis of the changes that have occurred in SARS-CoV-2 genomes from the global clinical population suggests the predominant driver of evolution in SARS-CoV-2 has been the accumulation of mutations resulting in increased transmissibility (Markov et al., 2023). Increased transmissibility is a multifaceted trait resulting from a given virus having an increased ability to survive within an infected individual, shed from an infected individual, establish within a new individual, or some combination of each of these abilities. These are all influenced by virus evading the host immune response. A range of 'key mutations' that are partially and additively responsible for each of these components of transmissibility have been identified. For example, several mutations in the Spike region have been linked to enhanced receptor binding, such as D614G, identified early in the pandemic (Yurkovetskiy et al., 2020), and N501Y, which was identified in several VOCs (Harvey et al., 2021; Leung et al., 2021; Liu et al., 2022). These conclusions predominantly based on clinical observations, albeit with further laboratory-based exploration, are valuable for understanding how the pandemic has unfolded and will continue to unfold.

Whilst genomic data derived from routine genomic sequencing for clinical or surveillance purposes (henceforth referred to as the "clinical population" of SARS-CoV-2) has enhanced understanding the evolution of SARS-CoV-2, there are inherent limitations in relying solely on this information. The availability of WGS data is influenced by differential sequencing efforts between countries, especially when routine WGS is difficult to achieve in low- and middle-income countries (Chen et al., 2022), or when data sharing in online repositories is not consistent among jurisdictions. Additionally, the gain or loss of mutations in these populations is affected by multiple uncontrolled processes including natural selection, genetic drift, host immunity, and population

dynamics. Understanding the relative impact of each process is difficult in such an uncontrolled environment. Consequently, it is challenging to understand the adaptation of SARS-CoV-2 to specific selective pressures, or to predict the potential evolutionary pathways, when relying solely on the clinical population.

Serial passaging *in vitro* provides complementary insights into the ongoing evolution of viruses. In these experiments, the virus is passaged through successive generations within a cell line, allowing study of virus evolution in a controlled setting, as mutations accumulate over time during the course of passaging (Holland et al., 1982). Most commonly, *in vitro* serial passaging is conducted to develop virus stocks and assess therapeutics (Dimmock and Easton, 2014), or to assess virus attenuation for vaccine development (Minor, 2015). Serial passaging can also be used to study the evolutionary trajectory of viruses over long term experiments, with strictly controlled time periods (Andino and Domingo, 2015; Bertels et al., 2019). These experiments can determine the speed at which a virus develops resistance to antiviral therapies, or to understand how the virus evolves over longer periods in the absence of selective constraints including immune pressure.

Few studies have investigated the evolutionary dynamics of SARS-CoV-2 over time *in vitro*. Based on limited passaging of ancestral lineages (<15 passages), it was reported that SARS-CoV-2 accumulates mutations readily *in vitro*, especially when passaged in Vero E6 cells, with an estimated *in vitro* spontaneous mutation rate of $1.3 \times 10^{-6} \pm 0.2 \times 10^{-6}$ per-base per-infection cycle (Amicone et al., 2021). These studies explicitly focusing on tracking the evolution of SARS-CoV-2 *in vitro* generally have studied a relatively small number of passages (e.g. <10), over a short time, and relatively few SARS-CoV-2 lineages. The greatest number of lineages published to date is 15 passages with two lineages from early in the pandemic (Amicone et al., 2021).

There is evidence for the convergent acquisition of mutations among samples taken through serial passage, even over small passage numbers, including some that have been observed in the global clinical population of SARS-CoV-2 (Chung et al., 2022). For example, a common observation is the accumulation of mutations associated with Vero E6-cultured samples (Amicone et al., 2021), especially in the furin cleavage site (PRRAR) within the S1/S2 domain of the SARS-CoV-2 spike glycoprotein. The furin cleavage site, noted early in the pandemic as an unusual characteristic of SARS-CoV-2 compared to other coronaviruses in the same clade (Coutard et al., 2020), has been proposed as a key component of the pathogenesis of SARS-CoV-2. Evidence suggests this sites has an important role in the affinity of SARS-CoV-2 for human hosts (Johnson et al., 2021). Deletion of the furin cleavage site has been linked with a fitness advantage in Vero E6 cells, albeit with this advantage reduced when ectopic expression of TMPRSS2 is introduced to the Vero E6 system (Johnson et al., 2021). Consequently, SARS-CoV-2 propagated in Vero E6 cell lines has been observed to repeatedly develop mutation(s) in the furin cleavage site, likely as an adaptation to the loss of the cell-surface serine protease-mediated cell entry mode since Vero E6 cells do not express TMPRSS2 (Aiewsakun et al., 2023). Accordingly, unintended selective pressures to develop alternative modes of cell entry can be imparted on Vero E6-propagated SARS-CoV-2, emphasising the need to interpret results in the context of known cell line-specific impacts.

Despite the insight gained from studies to date, further *in vitro* serial passaging studies of SARS-CoV-2 are needed to: i) more closely approach the multiple passages occurring the human population, ii) assess sites of mutation fixation, iii) use this assessment to determine potential antiviral and vaccine resistance sites developing in the absence of antiviral or vaccine pressure, and iv) inform therapeutic and vaccine research. In this study, we compared the accumulation of mutations *in vitro* in 11 different passaged viruses, corresponding to nine unique Pango lineages, throughout long-term serial passaging (33-100 passages per passaged virus line). The

evolutionary dynamics of these passage lines was determined by characterising the mutations that accumulated, both in terms of their number and potential functional consequences. Additionally, we assessed mutations for evidence of convergence across passage lines and/or with key mutations from the global clinical population of SARS-CoV-2.

Methods

Rationale and study design

Since the beginning of the COVID-19 pandemic, routine whole-genome sequencing (WGS) has been conducted at the Virology Research Laboratory, Serology and Virology Division (SAViD), NSW Health Pathology East, on PCR-positive SARS-CoV-2 clinical specimens. Viruses from clinical specimens were isolated *in vitro*, and then serially passaged and sequenced to investigate the evolutionary dynamics of SARS-CoV-2 in culture (see additional methods below). Initially an early variant (A.2.2) was chosen for this purpose. Later, additional lineages were also grown *in vitro* based on their relevance within the clinical population globally, with a particular focus on 'variants of concern' (VOC) or 'variants under investigation' (VUI), as designated by the World Health Organisation. In total, 11 different passage lines were established for the purpose of this study, with the sample details outlined in Table 1. All samples were taken through a minimum of 33 passages, up to a maximum of 100 passages.

Serial passaging

All SARS-CoV-2 cultures were performed in Vero E6s cells that were purchased commercially and have been verified by the ECACC (ECACC catalogue number 85020206). Vero E6 cells were maintained (up to a maximum of passage 30) in Minimum Essential Media supplemented with 10%-FBS and 1xPSG (MEM-10), and incubated at 37°C, 5% CO_2. The day prior to infection, a 24-well plate was seeded with 120,000 cells per well and incubated overnight, for approximately 90% confluency at the time of virus inoculation. The Vero E6 cell line was chosen as it supports viral replication to high titres due to its lack of interferon production and relatively high expression of the ACE-2 receptor (Emeny and Morgan, 1979). Therefore, using the Vero E6 cell line enabled viral replication dynamics to be observed in the absence of a host interferon response. The appearance of any immune evasion-associated mutations from the clinical population during in vitro passaging in Vero E6 cells can help to infer other fitness advantages of these mutations beyond immune evasion.

Clinical specimens (nasopharyngeal swabs in Virus Transport Media, referred to as "Passage 0") positive by diagnostic RT-qPCR were transported to a PC3 facility for virus culture. Specimens were spin-filtered (0.22 µm sterile Ultrafree-MC Centrifugal Filter) to remove cellular debris and reduce potential for bacterial and fungal contamination. Cell culture maintenance media was removed from wells, and 100 µL of virus-containing flow-through from spin-filtered specimens was added to wells. Plates were incubated for 1hr, before inoculum was removed and replaced with 500 µL maintenance media (MEM-2). Virus cultures were incubated for 3-4 days and observed for cytopathic effect (CPE). Cultured virus was then harvested (passage 1), diluted 1:1000, and used to inoculate a fresh plate of naïve Vero E6 cells (passage 2). This dilution was chosen for an estimated MOI of 0.01, based upon viral titres plateauing in Vero E6 cells at approximately $2x10^6$ TCID50/mL. Cultures of each SARS-CoV-2 lineage were maintained up to a maximum of passage 100. Aliquots of each virus passage were frozen at -80°C until later extraction for whole-genome sequencing.

Whole-genome sequencing

Samples were taken from each passage line and prepared for whole-genome sequencing (WGS). All wet laboratory methods follow those described previously (Foster et al., 2022), with the

exception of the choice of amplicon scheme. In the present study, amplification was performed using the “Midnight” protocol, comprising tiled 1200 nucleotide amplicons (Freed et al., 2020), followed by 150 bp paired-end sequencing on an Illumina MiSeq (Illumina Inc). Sequence was not obtained from every passage line, focussing on sequencing passages 0–6, then every three passages onwards where possible.

Quality control and variant calling

Sequencing data were processed and analysed using an in-house bioinformatics pipeline (“CIS”) (Foster, 2023). This leverages open-source bioinformatics tools for whole-genome sequencing, with workflow management controlled by Snakemake (Mölder et al., 2021). Description of the pipeline components relevant to this study are as follows. Briefly, initial QC of sequencing reads iis performed with fastp v0.23.2 (Chen et al., 2018), with removal of residual sequencing adapters, error correction, and filtration of reads based on a quality score threshold. Reads passing QC are then mapped against the SARS-CoV-2 reference genome (NC_045512.2) using bwa mem v0.7.17-r1188 (Li, 2013), and amplicon primer regions are soft-clipped using ivar v1.3.1 (Grubaugh et al., 2019). Probabilistic realignment of reads and variant calling is performed with lofreq v2.1.5 (Wilm et al., 2012). A consensus genome is assembled using bcftools v1.13 (Danecek et al., 2021), and coverage statistics estimated using bedtools v2.30.0 (Quinlan and Hall, 2010). Finally, Pango lineages are assigned using pangolin (O’Toole et al., 2021) and nextclade (Aksamentov et al., 2021), then relevant pipeline statistics and additional QC metrics by nextclade are incorporated into a final report. The pipeline is freely available from https://github.com/charlesfoster/covid-illumina-snakemake.

Several of the default parameters in the CIS pipeline were altered to align with the goals of this study. While the minimum depth of coverage for a variant to be called was retained at 10, we reduced the minimum SNP and indel variant allele frequency parameters to 0.01 (later filtered further, see below). While this allowed us to track low-frequency variants, we acknowledge that a lack of uniformity in the depth of coverage across the SARS-CoV-2 genome might impact upon the minimum callable variant allele frequency across sites. Consequently, there is a chance that some variants occurring at very low allele frequencies might be missed in areas of low depth of coverage, but this is a limitation when investigating low-frequency variants using whole-genome sequencing in general.

Tracking mutational changes during serial passaging

We assessed the changes in called variants within and among passage lines throughout serial passaging using our in-house “vartracker” pipeline (see below, available from https://github.com/charlesfoster/vartracker), using the variant call format (VCF) files from lofreq as input. For each passage sample within a passage line, these VCF files were derived by calling variants against the SARS-CoV-2 reference genome (using the CIS pipeline, as per above), not against the prior passage number. Doing so allows variants to be discussed using standard notation for SARS-CoV-2, while also allowing the gain and/or loss of variants between passages to be tracked.

The vartracker pipeline comprises a series of in-house python scripts to allow interrogation of the mutations that accumulate within a passage line during serial passaging. During the pipeline, the VCF files for each passage line were prefiltered to retain variants with a minimum single-nucleotide variant (SNV) and indel frequency 0.03 and 0.1, respectively, using cyvcf2 (Pedersen and Quinlan, 2017) and bcftools. Functional annotation of called variants was inferred using bcftools csq (Danecek and McCarthy, 2017), followed by merging into a single file. The merged VCF was then processed using custom python code to track the change in presence/absence of a given variant throughout the trajectory of the passage line (from passage 0 to the final passage),

as well as the change in allele frequency of each variant throughout passaging. Variants were classified under four main broad categories: present in passage 0 but lost throughout passaging ('original_lost'), present in passage 0 and retained throughout passaging ('original_retained'), absent in passage 0 but gained and retained throughout passaging ('new_persistent'), or absent in passage 0 but gained and lost throughout passaging ('new_transient'). All variants were also subject to a suite of quality control measures incorporating the estimated variant depth, the overall site depth, the depth in a window of sites surrounding the variant site, and an overall metric.

We investigated convergent evolution of any new_persistent or new_transient variants among passage lines. For the purposes of this study, we defined convergence as (a) any case where any two (or more) replicates obtained the same mutation independently during the course of serial passaging, or (b) any passage line developed a mutation recognised as clinically significant within the global population of SARS-CoV-2 based on searches against a database of SARS-CoV-2 mutations comprising information on the functional consequences of mutations (Anwar et al., 2022). Additionally, we calculated the rate of mutation accumulation within each passage line, considering the rate among the overall genome as well as individual genes/regions within the genome, using the following formula: $M_a(r) = \frac{\Sigma f_r}{P.L_r}$ (following the approach of (Amicone et al., 2021)). In this formula, Σf_r is the sum of the frequency of all detected mutations in a region r, P is the number of passages, and L_r is the length of r. We calculated the rate for each applicable passage up to and including passage 33 to observe whether the inferred mutation rate varies over time.

We investigated the evolutionary dynamics within all passage lines from passage 0, or the earliest passage successfully sequenced, until their final passage number (Table 1). However, for all comparisons among passage lines, we restricted our focus to passages 0–33, with passage 33 representing the maximum passage number in common that all passage lines had reached. We also investigated in further detail the evolutionary trajectory of passage line "POW005" (Pango lineage: B.1.319), which has been maintained for the greatest number of passages (100) across all passage lines. The full results for all other passage lines across all passages are not discussed in this manuscript, but are available within the supplementary materials (Table S2). It is also worth noting that sequencing data for some passage numbers from some passage lines are not available. In these cases, particularly with samples corresponding to VOCs, there was insufficient material from the early passages to conduct WGS and/or the material was needed for unrelated neutralization assay studies.

Phylogenetic analysis

A phylogenetic tree was estimated to investigate further the evolution of the passaged virus lines *in vitro*. All isolate consensus genomes were aligned against the Wuhan Hu-1 reference genome using minimap2 (Li, 2018), followed by trimming of the 5' and 3' UTRs and conversion to multifasta format using gofasta (Jackson, 2022). We then used an in-house script to mask known problematic sites from the alignment (De Maio et al., 2020), and filtered out sites with too many gaps using esl-alimask (hmmer.org). Finally, we inferred a maximum likelihood phylogeny for the samples using iqtree2 (Nguyen et al., 2015), with the best fitting nucleotide substitution model chosen using a constrained search using ModelFinder ('mset': GTR, TIM2, GTR; 'mfreq': F; 'mrate': 'G,R') (Kalyaanamoorthy et al., 2017), and support estimated using 1000 ultrafast bootstraps (Hoang et al., 2018).

Results and Discussion

Sequencing metrics

The majority of samples from each passage line were successfully sequenced (Supplementary Table S1). Excluding one sample that yielded no sequence, the mean reference genome coverage at a depth of at least 10 reads was 99.19% (SD: 1.07). Each of these samples was also sequenced at a high mean depth (mean 1334.48, SD: 753). All except one passage line were called as the same lineage as their original isolate (passage 0) after their maximum number of passages. The exception was "POW005", which was originally called as the lineage B.1.319, but from passage 5 onwards was called as B.1 by pangolin, albeit with conflicting placements by Usher (B.1(1/3); B.1.319(1/3); B.1.616(1/3)). However, Nextclade called the lineage of passage POW005 as B.1.319 from passage 0 through to passage 100, despite the accumulation of many private mutations. The number of sequenced passages varied between passage lines (Table 1), including up to 100 passages for "POW005" (see below). We provide the sequencing reads and results for all passage numbers for all passage lines in case they are of use to the scientific community (Supplementary Table S1–2). However, for the purposes of this manuscript all comparisons among passage lines are discussed based on a maximum of 33 passages. This cap was chosen to allow a fair common point of comparison among passage lines despite a difference in passaging and sequencing efforts. The full range of sequencing results for 100 passages of POW005 are still discussed, albeit without comparison to other passage lines.

Evolutionary dynamics across passage lines *in vitro*

After more than three and a half years of the COVID-19 pandemic, SARS-CoV-2 continues to diversify at a remarkable rate in the global clinical population. We found that SARS-CoV-2 steadily accumulated mutations *in vitro* throughout most of its genome with fluctuating variant allele frequencies (VAFs), reflecting what continues to occur in the clinical population (Figure 1, Supplementary Table S2). Many of these mutations were detected at a very low VAF within a given passage (e.g., <5%) and were then lost in subsequent passages. Conversely, some new mutations that arose during passaging persisted until the final passage and became near-fixed at a consensus-level frequency (Figure 2, Supplementary Table S2. Supplementary Figures S1–S26). Most variants (~90%) relative to the Wuhan Hu-1 reference genome present in passage 0 of a given passage line were retained during the course of serial passaging. Occasionally these 'original' variants were lost, most commonly when they were originally present at a sub-consensus level, but sometimes even when well supported (allele frequency >50%, ~2% of all variants). Variants were detected in all genes of the SARS-CoV-2 genome but occurred at different frequencies among genes and among passage lines (Figures 2–3, Supplementary Figures S1–26).

The accumulation of mutations over time was reflected in a gradual divergence between passage 0 and the final passage *within* each passage line, but without significantly affecting the phylogenetic relationships between passage lines (Figure 4). Nearly all samples within a given passage line form clades exclusive of the other passage lines, with the only exceptions being some poorly supported relationships among POW003 and POW007 (both of the A.2.2 Pango lineage). These results demonstrate that the convergent acquisition of some mutations among passage lines (as discussed below) did not impact upon inferred phylogenetic relationships. Overall, the phylogenetic relationships among passage lines reflects the expected topology based on the relationships among SARS-CoV-2 lineages within the global phylogeny. The inferred mutation rates *in vitro* varied among passage lines and varied within passage lines over time (Figure 5). There was a more than threefold difference in mutation rate between the passage lines with the greatest (Delta; ~8.51 x 10^{-05} mutations per passage per nucleotide) and smallest ("POW004";

~2.64 x 10^{-05} mutations per passage per nucleotide) mutation rates. In general, across passage lines there was a trend to a reduced mutation rate as the number of serial passages increased.

No plateau after 100 serial passages

The "POW005" (Pango lineage: B.1.319) passage line was carried through the greatest number of passages across all passage lines in this study. There was a continuous accumulation of mutations in this passage line throughout the course of serial passaging, even up to passage 100 (Figure 6, Supplementary Table S2). The initial (passage 0) isolate possessed 10 variants relative to the Wuhan Hu-1 reference genome: one in the 5' UTR and nine occurring in coding regions, of which eight were present as the majority allele and seven were non-synonymous variants. Throughout the course of serial passaging, POW005 accumulated 131 new variants (58 missense including two in-frame deletions, 63 synonymous, 10 in intergenic regions/UTRs), of which 97 were transient and 34 persisted until passage 100. The sole low-frequency variant detected in passage 0 was lost during passaging, although the other 10 variants present at passage 0 were retained. The passage line was still readily replicating with no obvious signs of impaired fitness, demonstrating the long-term viability of SARS-CoV-2 *in vitro* despite a frequent mutation accumulation.

Mutations by gene location

Previous studies have concluded that the spike region of SARS-CoV-2 is a mutational hotspot. Whilst we observed many mutations arising in the spike gene (Figure 2), after correcting for gene length, the number of mutations in the spike gene was comparable with that of other genes (Figure 3). Genes coding for other structural and accessory proteins (e.g. M, ORF7a, ORF7b) accumulated mutations at a greater rate than other regions, including spike, with variation between passage lines (Figure 3). While the spike region is clearly an important region of the SARS-CoV-2 genome for mutation, our results further reflect recent studies highlighting the importance of other regions of the genome for understanding the ongoing evolution of SARS-CoV-2 (Arshad et al., 2023; Foster et al., 2023; Redondo et al., 2021; Zandi et al., 2022), and the capacity of the virus to adapt to new evolutionary pressures.

Signatures of convergent evolution

A hallmark of the COVID-19 pandemic has been high levels of homoplasy most likely caused by convergent and parallel evolution. Even from early within the pandemic, sites within the SARS-CoV-2 genome were noted as being highly homoplastic and recommended to be masked from alignments when estimating phylogenies (De Maio et al., 2020). As the pandemic has progressed, multiple mutations speculated to impart fitness benefits on SARS-CoV-2 have been observed. For example, the spike mutations N501Y, E484K and ΔH69/V70 have arisen several times independently in lineages designated as variants of concern, and are proposed to lead to increased immune escape and/or increased ACE2 binding affinity (Harvey et al., 2021). Therefore, to understand further the impact of the mutations arising *de novo* during long-term passaging, we determined whether there were any signatures of convergent evolution.

Although the majority of variants arising during serial passaging were passage-line specific, there were also many cases where different passage lines independently acquired the same variants in a convergent manner. In total, there were 13 variants that arose throughout serial passaging whereby (a) the mutation was present in two or more passage lines, and (b) the mutation newly arose in at least one of the passage lines (Table 2). Generally, these mutations only appeared at a low frequency in few passage lines, but occasionally went to fixation in multiple passage lines. Some convergent mutations were expected to arise given that they have been noted repeatedly to arise during serial passaging in Vero E6 cells, especially in the region of the spike furin-cleavage site (Ogando et al., 2020; Sasaki et al., 2021). For example, the S:YQTQTN674Y mutation, a deletion of five amino acids near the spike S1/S2 cleavage site, arose independently in POW003 (A.2.2), POW005 (B.1.319) and POW007 (A.2.2). This same mutation

emerged multiple times in two background lineages in a previous study (Amicone et al., 2021). We also observed four different missense amino acid replacements proximal to the furin-cleavage site at amino acid position 682 of spike (R682G, R682W, R682L, R682Q) at varying allele frequencies, as well as a six amino acid deletion in one passage line (RARSVA683R). All but one of these mutations appeared within four serial passages.

The clinical significance of the mutations was important, for example because of their noted impacts on transmissibility or disease severity on serial passaging *in vivo*. Any mutations associated with enhanced virus replication *in vitro* would be expected to be beneficial for virus survival and selected for, as is the case with replication-enhancing mutations in the clinical population. For example, the emergence of the spike mutation D614G early in the COVID-19 pandemic was linked with the proliferation of virus with enhanced replication (Zhou et al., 2021). Additional changes in the spike region have been linked to enhanced virus replication at subsequent stages of the pandemic, such as the P681R mutation within the Delta VOC (Saito et al., 2022). However, the impact of mutations in other genomic regions on virus replication is also important to consider. A well characterised pair of sequential non-synonymous amino acid changes in the nucleocapsid gene, N:R203K and N:G204R, augment virus replication in SARS-CoV-2 (Johnson et al., 2022). Comparing our results with a curated database of SARS-CoV-2 mutations revealed that there were many cases where clinically significant mutations arose during serial passaging. At least 16 different variants that arose during serial passaging have important functional consequences in the global clinical population of SARS-CoV-2, as recorded under 54 functional categories (19 unique) in a compendium of scientific literature (Anwar et al., 2022) (Table 3). Noted functional impacts of the newly arising mutations in our study, including the spike mutations L5F, A67V, T76I, A222V and others, are related to various aspects of pharmaceutical effectiveness, including vaccine efficacy and antibody neutralization (Table 3).

Previous research that took a replication-deficient murine hepatitis virus (MHV, a coronavirus) through 250 serial passages showed evidence of selection for increased replication fidelity and reduced susceptibility to nucleoside analogues over time (Graepel et al., 2017), explained partially by secondary mutations in nsp12 and nsp14. While the passage 0 viruses of each of our passage lines were not replication-deficient, albeit with potential differences in replication efficiency between the various SARS-CoV-2 lineages we sampled, we explored our results to determine whether any mutations arose with the potential to impact replication fidelity. In particular, we focused on nsp5 (protease, $3CL^{pro}$, target of lopinavir and nirmatrelvir), nsp10 (cofactor that stimulates ExoN), nsp12 (RNA-dependent RNA polymerase, RdRp, target of remdesivir, favipiravir and molnupiravir), and nsp14 (exonuclease, ExoN). We found 15 non-synonymous mutations in these regions, some of which became the majority allele and/or went to fixation (Table 4). Of these, several have previously been linked to altered replication and/or resistance to antivirals that target SARS-CoV-2 replication. Within nsp14, the P203L mutation, which arose at a low VAF in passage line POW007, has been linked previously to altered replication (Takada et al., 2023). Additionally, the nsp14:A504V mutation that arose in our passage line of the Alpha variant has been demonstrated clinically to temporally associate with remdesivir resistance (Gandhi et al., 2022). The T21I and P252L mutations that arose within nsp5 have been determined to be precursor mutations in several common mutational pathways to nirmatrelvir resistance (Iketani et al., 2023). None of the newly arising mutations in nsp10 and nsp12 have been explicitly linked thus far with altered replication dynamics, but one (nsp10:T49I) arose through serial passaging during development of an inactivated vaccine candidate for SARS-CoV-2 (Gao et al., 2020), and others (e.g. nsp12:D92A and T293I) have arisen independently in the global clinical population without a clear indication of their functional consequences.

The repeated evolution of these clinically significant mutations conclusively demonstrates that variants that are related to immune evasion can arise during *in vitro* serial passaging even in the absence of immune or drug-related selective pressures. This is because (a) we passaged the viruses through a Vero E6 cell line, which lacks an innate immune response, and (b) we did not directly apply any selective agents to the samples during passaging, such as neutralising antibodies. This result raises the possibility that (at least some) mutations associated with immune escape that arose in the clinical population were not driven by intra-host selection in the presence of (e.g.) antiviral therapies (cf. Weigang et al. (2021)), but instead arose *de novo* with intrinsic immune escape benefits. However, it is possible that there could be another benefit of these putative immune-related mutations to the survival of SARS-CoV-2 outside of escaping an immune response.

We also observed the loss of at least one clinically significant mutation throughout the course of serial passaging. One key variant hypothesised to have contributed to the success of the Omicron BA.1 lineage is S:S375F, a mutation within the receptor-binding domain of the Spike protein responsible for attenuation of spike cleavage efficiency and fusogenicity as well as decreased ACE2 binding affinity (Kimura et al., 2022). This key mutation was present in our BA.1 passage line at a VAF of ~1 from passage 0 until passage 6 (i.e., fixed as the majority allele), but was only present at a low VAF of 13% in passage 9, and was then not detected in subsequent passages (Supplementary Table S2). The dominance of S:S375F in global Omicron sequences suggests the site may have been subject to initial positive selection followed by purifying selection to retain benefits imparted by the mutation. However, its loss throughout serial passaging suggests that the benefits in the clinical population do not translate to *in vitro* benefits, at least in Vero E6 cell lines.

A putative rapid switch in cell entry pathway *in vitro*

The most striking example of convergent evolution across passage lines was the evolution of S:H655Y on repeated occasions (Figure 2). This mutation was already present in passage 0 in two passage lines, and arose newly throughout serial passaging in six of the remaining nine passage lines. The S:H655Y mutation was originally detected in early cases of the Gamma and Omicron VOCs. Impacts of the S:H655Y mutation include acting as a “gateway” mutation by increasing the fitness of lineages with complex combinations of clinically significant mutations, and increased spike cleavage and fusogenicity associated with enhancement of the endosomal cell entry pathway (Yamamoto et al., 2022; Yurkovetskiy et al., 2020). A putative switch towards preferentially using an endosomal cell entry pathway within our passage lines, rather than the ACE2-TMPRSS2 pathway typical of most variants prior to Omicron (Jackson et al., 2022), is not surprising given that Vero E6 cell lines do not express TMPRSS2. Similar changes in virus tropism have been observed in the clinical population. For example, several lineages of the Omicron BA.1 and BA.2 variants (and their descendants) used an endosomal cell entry pathway rather than the ACE2-TMPRSS2 pathway for virus entry (Aggarwal et al., 2022). This change in tropism resulted in Omicron replicating more efficiently in the bronchi, but not productively infecting human alveolar type 2 cells of the lung (Hui et al., 2022; Lamers et al., 2022). These changes, among other factors, likely contributed to the high transmissibility and decreased pathogenicity observed clinically since the emergence of Omicron and its sub-lineages (Hyams et al., 2023; Yuan et al., 2022).

Adaptation, bottlenecks and genetic drift

The success of the various lineages of SARS-CoV-2 in spreading through the human population has been linked to functional effects of mutations that accrue over time (Markov et al., 2023). Determining why some mutations go on to be fixed, whereas others are temporary, is important to understand the evolutionary trajectory of SARS-CoV-2. In general, positive selection has played an

important role in the COVID-19 pandemic. For example mutations aiding in immune escape have been selected for in a chronically infected host, particularly if that host is immune compromised. This process is hypothesised to have led to the emergence of variants of concern such as Omicron (Viana et al., 2022). Positive selection of mutations has been observed to arise during serial passaging in cell lines (Amicone et al., 2021), as well as in animal models such as minks or domestic cats (Bashor et al., 2022; Shuai et al., 2020).

We observed many variants newly arising in all passaged SARS-CoV-2 lineages (Figures 1–2, 6–7; Supplementary Figures S1–26; Supplementary Table S2). Some of the >170 newly arising variants were transient and purged from the virus populations throughout the course of serial passaging, but some persisted until the final serial passages, occasionally at (near-) fixation within the virus populations. One signature of positive selection is a selective sweep, whereby a rare or previously non-existing allele rapidly increases in frequency within a population. Therefore, we considered the fixation of these newly arising mutations throughout the course of serial passaging to represent possible positive selection for mutations beneficial to virus survival *in vitro.* Examples include the furin cleavage site-associated mutations and mutations associated with a change in cell entry pathway (discussed above).

An alternative cause of the many mutations accumulating during serial passaging is genetic drift. In the absence of positive selection for beneficial mutations and/or strong negative selection, which reduces the selective pressure against deleterious alleles, alleles may proliferate by chance through genetic drift (Lahti et al., 2009). Consequently, although many mutations we observed have previously been linked to changes in the efficacy of vaccines and/or other pharmaceuticals (e.g. the spike, nsp5 and nsp14 mutations discussed above), they could have arisen and been successful through chance alone, such as through transmission bottlenecks between successive serial passages. Indeed, a factor potentially influencing our results is that our serial passaging protocol was designed to maintain an estimated MOI of 0.01, allowing for cytopathic effects to become evident within a reasonable time frame before passaging continued. Maintaining a lower virus titre during serial passaging can increase the impact of genetic bottlenecks, influencing the fate of emerging variants and potentially obscuring whether changes in variant frequency were driven by adaptation or stochastic events like genetic drift (Duffy et al., 2008; Lauring and Andino, 2010; Moya et al., 2004). One putative case of an abrupt shift in variant allele frequencies caused by a genetic bottleneck can be observed in the POW003 (A.2.2) passage line, whereby there was an abrupt loss and gain of several variants between passages 24 and 27 (Figure 7). However, given that our intention was to track to the accumulation and/or loss of variants in vitro regardless of the mechanism driving any changes, whether selection, drift, or otherwise, we do not consider this to have affected results here. Analogous situations in the global clinical populations of SARS-CoV-2 have been observed, whereby mutations that were either non-beneficial, or potentially even mildly deleterious, became fixed within given regions after public health measures created transmission bottlenecks (e.g. (Foster et al., 2023)). Likewise, the ORF8 accessory region remains a hotspot for mutations throughout the COVID-19 pandemic (Arduini et al., 2023; Hisner et al., 2023), possibly as a result of a relaxation of purifying selection, as was hypothesised for SARS-CoV (Zinzula, 2021).

Concluding remarks

Our study comprehensively explores the *in vitro* evolutionary dynamics of SARS-CoV-2 using the greatest number of serial passages in similar SARS-CoV-2 research to date. In addition to generating a wealth of genomic data for the scientific community to explore, our results demonstrate the long-term capacity of SARS-CoV-2 to readily accumulate mutations *in vitro* in the Vero E6 cell line despite the inherent strong proofreading capacities of coronaviruses. As suggested by some studies from shorter-term serial passaging, we showed that that some of these

mutations (e.g. in the furin cleavage site) are relatively predictable. Additionally, we show that even after 100 serial passages SARS-CoV-2 continues to replicate readily with no apparent attenuation or decrease of fitness of the virus. Many variants that arose during serial passaging were convergent among passage lines and with the global clinical population of SARS-CoV-2, including some variants associated with altered therapeutic effectiveness (despite no treatment with antivirals during passaging). For example, mutations accumulated in regions associated with maintenance of replication fidelity (e.g. nsp12, nsp14), which can impact upon any therapeutics targeting these regions. Apart from revealing signatures of convergence with previously noted mutations of interest, our results provide a resource for investigating future changes occurring in SARS-CoV-2 globally. Any mutations arising convergently among passage lines that have not been noted previously as occurring commonly during serial passaging, or in the global clinical population, are worth further investigation. The repeated appearance of these mutations during in vitro culture implies they benefit SARS-CoV-2, at least in vitro, and could also add to the growing list of Vero E6-associated mutations in SARS-CoV-2. The same is true for other mutations arising de novo even in a single passage line.

Data availability

The consensus genomes of all passage 0 samples from this study have been uploaded to GISAID (see Table 1), and all sequence data have been uploaded to NCBI's GenBank Sequence Read Archive under accession number PRJNA1018257. The pipeline to process and analyse raw sequencing reads is available from https://github.com/charlesfoster/covid-illumina-snakemake, and the pipeline to summarise longitudinal variant calling results is available from https://github.com/charlesfoster/vartracker.

References

Aggarwal, A., Akerman, A., Milogiannakis, V., Silva, M.R., Walker, G., Stella, A.O., Kindinger, A., Angelovich, T., Waring, E., Amatayakul-Chantler, S., Roth, N., Manni, S., Hauser, T., Barnes, T., Condylios, A., Yeang, M., Wong, M., Jean, T., Foster, C.S.P., Christ, D., Hoppe, A.C., Munier, M.L., Darley, D., Churchill, M., Stark, D.J., Matthews, G., Rawlinson, W.D., Kelleher, A.D., Turville, S.G., 2022. SARS-CoV-2 Omicron BA.5: Evolving tropism and evasion of potent humoral responses and resistance to clinical immunotherapeutics relative to viral variants of concern. eBioMedicine 84, 104270. https://doi.org/10.1016/j.ebiom.2022.104270

Aiewsakun, P., Phumiphanjarphak, W., Ludowyke, N., Purwono, P.B., Manopwisedjaroen, S., Srisaowakarn, C., Ekronarongchai, S., Suksatu, A., Yuvaniyama, J., Thitithanyanont, A., 2023. Systematic Exploration of SARS-CoV-2 Adaptation to Vero E6, Vero E6/TMPRSS2, and Calu-3 Cells. Genome Biol Evol 15, evad035. https://doi.org/10.1093/gbe/evad035

Aksamentov, I., Roemer, C., Hodcroft, E.B., Neher, R.A., 2021. Nextclade: clade assignment, mutation calling and quality control for viral genomes. Journal of Open Source Software 6, 3773. https://doi.org/10.21105/joss.03773

Amicone, M., Borges, V., Alves, M.J., Isidro, J., ZÃ©-ZÃ©, L., Duarte, S., Vieira, L., Guiomar, R., Gomes, J.P., Gordo, I., 2021. Mutation rate of SARS-CoV-2 and emergence of mutators during experimental evolution. https://doi.org/10.1101/2021.05.19.444774

Andino, R., Domingo, E., 2015. Viral quasispecies. Virology, 60th Anniversary Issue 479–480, 46–51. https://doi.org/10.1016/j.virol.2015.03.022

Anwar, M.Z., Gill, I.S., Iseminger, M., Sehar, A., Igwacho, K.D., Vora, K., Domselaar, G.V., Gordon, P.M.K., Hsiao, W.W., 2022. COVID-MVP: an interactive visualization for tracking SARS-CoV-2 mutations, variants, and prevalence, enabled by curated functional annotations and portable genomics workflow. bioRxiv 2022.06.07.493653. https://doi.org/10.1101/2022.06.07.493653

Arduini, A., Laprise, F., Liang, C., 2023. SARS-CoV-2 ORF8: A Rapidly Evolving Immune and Viral Modulator in COVID-19. Viruses 15, 871. https://doi.org/10.3390/v15040871

Arshad, N., Laurent-Rolle, M., Ahmed, W.S., Hsu, J.C.-C., Mitchell, S.M., Pawlak, J., Sengupta, D., Biswas, K.H., Cresswell, P., 2023. SARS-CoV-2 accessory proteins ORF7a and ORF3a use distinct mechanisms to down-regulate MHC-I surface expression. Proceedings of the National Academy of Sciences 120, e2208525120. https://doi.org/10.1073/pnas.2208525120

Bashor, L., Gagne, R.B., Bosco-Lauth, A., Stenglein, M., VandeWoude, S., 2022. Rapid evolution of SARS-CoV-2 in domestic cats. Virus Evolution 8, veac092. https://doi.org/10.1093/ve/veac092

Bertels, F., Leemann, C., Metzner, K.J., Regoes, R.R., 2019. Parallel Evolution of HIV-1 in a Long-Term Experiment. Molecular Biology and Evolution 36, 2400–2414. https://doi.org/10.1093/molbev/msz155

Chen, S., Zhou, Y., Chen, Y., Gu, J., 2018. fastp: an ultra-fast all-in-one FASTQ preprocessor. Bioinformatics 34, i884–i890. https://doi.org/10.1093/bioinformatics/bty560

Chen, Z., Azman, A.S., Chen, X., Zou, J., Tian, Y., Sun, R., Xu, X., Wu, Y., Lu, W., Ge, S., Zhao, Z., Yang, J., Leung, D.T., Domman, D.B., Yu, H., 2022. Global landscape of SARS-CoV-2 genomic surveillance and data sharing. Nat Genet 54, 499–507. https://doi.org/10.1038/s41588-022-01033-y

Chung, H., Noh, J.Y., Koo, B.-S., Hong, J.J., Kim, H.K., 2022. SARS-CoV-2 mutations acquired during serial passage in human cell lines are consistent with several of

those found in recent natural SARS-CoV-2 variants. Computational and Structural Biotechnology Journal 20, 1925–1934. https://doi.org/10.1016/j.csbj.2022.04.022
Coutard, B., Valle, C., de Lamballerie, X., Canard, B., Seidah, N.G., Decroly, E., 2020. The spike glycoprotein of the new coronavirus 2019-nCoV contains a furin-like cleavage site absent in CoV of the same clade. Antiviral Research 176, 104742. https://doi.org/10.1016/j.antiviral.2020.104742
Danecek, P., Bonfield, J.K., Liddle, J., Marshall, J., Ohan, V., Pollard, M.O., Whitwham, A., Keane, T., McCarthy, S.A., Davies, R.M., Li, H., 2021. Twelve years of SAMtools and BCFtools. GigaScience 10. https://doi.org/10.1093/gigascience/giab008
Danecek, P., McCarthy, S.A., 2017. BCFtools/csq: haplotype-aware variant consequences. Bioinformatics 33, 2037–2039. https://doi.org/10.1093/bioinformatics/btx100
De Maio, N., Walker, C., Borges, R., Weilguny, L., Slodkowicz, G., Goldman, N., 2020. Issues with SARS-CoV-2 sequencing data [WWW Document]. Virological. URL https://virological.org/t/issues-with-sars-cov-2-sequencing-data/473 (accessed 4.14.21).
Dimmock, N.J., Easton, A.J., 2014. Defective Interfering Influenza Virus RNAs: Time To Reevaluate Their Clinical Potential as Broad-Spectrum Antivirals? Journal of Virology 88, 5217–5227. https://doi.org/10.1128/jvi.03193-13
Duffy, S., Shackelton, L.A., Holmes, E.C., 2008. Rates of evolutionary change in viruses: patterns and determinants. Nat Rev Genet 9, 267–276. https://doi.org/10.1038/nrg2323
Emeny, J.M., Morgan, M.J., 1979. Regulation of the interferon system: evidence that Vero cells have a genetic defect in interferon production. J Gen Virol 43, 247–252. https://doi.org/10.1099/0022-1317-43-1-247
Foster, C.S.P., 2023. covid-illumina-snakemake: a pipeline to facilitate genomic surveillance of SARS-CoV-2. https://doi.org/10.5281/zenodo.8253928
Foster, C.S.P., Bull, R.A., Tedla, N., Santiago, F., Agapiou, D., Adhikari, A., Walker, G.J., Shrestha, L.B., Van Hal, S.J., Kim, K.W., Rawlinson, W.D., 2023. Persistence of a Frameshifting Deletion in SARS-CoV-2 ORF7a for the Duration of a Major Outbreak. Viruses 15, 522. https://doi.org/10.3390/v15020522
Foster, C.S.P., Stelzer-Braid, S., Deveson, I.W., Bull, R.A., Yeang, M., Au, J.-P., Ruiz Silva, M., van Hal, S.J., Rockett, R.J., Sintchenko, V., Kim, K.W., Rawlinson, W.D., 2022. Assessment of Inter-Laboratory Differences in SARS-CoV-2 Consensus Genome Assemblies between Public Health Laboratories in Australia. Viruses 14, 185. https://doi.org/10.3390/v14020185
Freed, N.E., Vlková, M., Faisal, M.B., Silander, O.K., 2020. Rapid and inexpensive whole-genome sequencing of SARS-CoV-2 using 1200 bp tiled amplicons and Oxford Nanopore Rapid Barcoding. Biology Methods and Protocols 5, bpaa014. https://doi.org/10.1093/biomethods/bpaa014
Gandhi, S., Klein, J., Robertson, A.J., Peña-Hernández, M.A., Lin, M.J., Roychoudhury, P., Lu, P., Fournier, J., Ferguson, D., Mohamed Bakhash, S.A.K., Catherine Muenker, M., Srivathsan, A., Wunder, E.A., Kerantzas, N., Wang, W., Lindenbach, B., Pyle, A., Wilen, C.B., Ogbuagu, O., Greninger, A.L., Iwasaki, A., Schulz, W.L., Ko, A.I., 2022. De novo emergence of a remdesivir resistance mutation during treatment of persistent SARS-CoV-2 infection in an immunocompromised patient: a case report. Nat Commun 13, 1547. https://doi.org/10.1038/s41467-022-29104-y
Gao, Q., Bao, L., Mao, H., Wang, L., Xu, K., Yang, M., Li, Yajing, Zhu, Ling, Wang, N., Lv, Z., Gao, H., Ge, X., Kan, B., Hu, Y., Liu, J., Cai, F., Jiang, D., Yin, Y., Qin, Chengfeng, Li, J., Gong, X., Lou, X., Shi, W., Wu, D., Zhang, H., Zhu, Lang, Deng, W., Li, Yurong, Lu, J., Li, C., Wang, X., Yin, W., Zhang, Y., Qin, Chuan, 2020. Development of an inactivated vaccine candidate for SARS-CoV-2. Science 369, 77–81. https://doi.org/10.1126/science.abc1932

Graepel, K.W., Lu, X., Case, J.B., Sexton, N.R., Smith, E.C., Denison, M.R., 2017. Proofreading-Deficient Coronaviruses Adapt for Increased Fitness over Long-Term Passage without Reversion of Exoribonuclease-Inactivating Mutations. mBio 8, 10.1128/mbio.01503-17. https://doi.org/10.1128/mbio.01503-17

Grubaugh, N.D., Gangavarapu, K., Quick, J., Matteson, N.L., De Jesus, J.G., Main, B.J., Tan, A.L., Paul, L.M., Brackney, D.E., Grewal, S., Gurfield, N., Van Rompay, K.K.A., Isern, S., Michael, S.F., Coffey, L.L., Loman, N.J., Andersen, K.G., 2019. An amplicon-based sequencing framework for accurately measuring intrahost virus diversity using PrimalSeq and iVar. Genome Biology 20, 8. https://doi.org/10.1186/s13059-018-1618-7

Harvey, W.T., Carabelli, A.M., Jackson, B., Gupta, R.K., Thomson, E.C., Harrison, E.M., Ludden, C., Reeve, R., Rambaut, A., Peacock, S.J., Robertson, D.L., 2021. SARS-CoV-2 variants, spike mutations and immune escape. Nat Rev Microbiol 19, 409–424. https://doi.org/10.1038/s41579-021-00573-0

Hisner, R., Gueli, F., Peacock, T., 2023. Repeated loss of ORF8 expression in circulating SARS-CoV-2 lineages - SARS-CoV-2 coronavirus. Virological.

Hoang, D.T., Chernomor, O., von Haeseler, A., Minh, B.Q., Vinh, L.S., 2018. UFBoot2: Improving the Ultrafast Bootstrap Approximation. Molecular Biology and Evolution 35, 518–522. https://doi.org/10.1093/molbev/msx281

Holland, J., Spindler, K., Horodyski, F., Grabau, E., Nichol, S., VandePol, S., 1982. Rapid Evolution of RNA Genomes. Science 215, 1577–1585. https://doi.org/10.1126/science.7041255

Hui, K.P.Y., Ho, J.C.W., Cheung, M., Ng, K., Ching, R.H.H., Lai, K., Kam, T.T., Gu, H., Sit, K.-Y., Hsin, M.K.Y., Au, T.W.K., Poon, L.L.M., Peiris, M., Nicholls, J.M., Chan, M.C.W., 2022. SARS-CoV-2 Omicron variant replication in human bronchus and lung ex vivo. Nature 603, 715–720. https://doi.org/10.1038/s41586-022-04479-6

Hyams, C., Challen, R., Marlow, R., Nguyen, J., Begier, E., Southern, J., King, J., Morley, A., Kinney, J., Clout, M., Oliver, J., Gray, S., Ellsbury, G., Maskell, N., Jodar, L., Gessner, B., McLaughlin, J., Danon, L., Finn, A., Morley, A., Langdon, A., Turner, A., Mattocks, A., Osborne, B., Grimes, C., Mitchell, C., Adegbite, D., Bridgeman, E., Scott, E., Perkins, F., Bayley, F., Ruffino, G., Valentine, G., Tilzey, G., Campling, J., Wright, J.K., Brzezinska, J., Cloake, J., Milutinovic, K., Helliker, K., Maughan, K., Fox, K., Minou, K., Ward, L., Fleming, L., Morrison, L., Smart, L., Wright, L., Grimwood, L., Bellavia, M., Clout, M., Vasquez, M., Gonzalez, M.G., Jeenes-Flanagan, M., Chang, N., Grace, N., Manning, N., Griffiths, O., Croxford, P., Sequenza, P., Lazarus, R., Walters, R., Marlow, R., Heath, R., Antico, R., Arachchge, S.N., Suppiah, S., Mona, T., Riaz, T., Mackay, V., Maseko, Z., Taylor, Z., Friedrich, Z., Szasz-Benczur, Z., 2023. Severity of Omicron (B.1.1.529) and Delta (B.1.617.2) SARS-CoV-2 infection among hospitalised adults: a prospective cohort study in Bristol, United Kingdom. The Lancet Regional Health – Europe 25. https://doi.org/10.1016/j.lanepe.2022.100556

Iketani, S., Mohri, H., Culbertson, B., Hong, S.J., Duan, Y., Luck, M.I., Annavajhala, M.K., Guo, Y., Sheng, Z., Uhlemann, A.-C., Goff, S.P., Sabo, Y., Yang, H., Chavez, A., Ho, D.D., 2023. Multiple pathways for SARS-CoV-2 resistance to nirmatrelvir. Nature 613, 558–564. https://doi.org/10.1038/s41586-022-05514-2

Jackson, B., 2022. gofasta: command-line utilities for genomic epidemiology research. Bioinformatics 38, 4033–4035. https://doi.org/10.1093/bioinformatics/btac424

Jackson, C.B., Farzan, M., Chen, B., Choe, H., 2022. Mechanisms of SARS-CoV-2 entry into cells. Nat Rev Mol Cell Biol 23, 3–20. https://doi.org/10.1038/s41580-021-00418-x

Johnson, B.A., Xie, X., Bailey, A.L., Kalveram, B., Lokugamage, K.G., Muruato, A., Zou, J., Zhang, X., Juelich, T., Smith, J.K., Zhang, L., Bopp, N., Schindewolf, C., Vu, M.,

Vanderheiden, A., Winkler, E.S., Swetnam, D., Plante, J.A., Aguilar, P., Plante, K.S., Popov, V., Lee, B., Weaver, S.C., Suthar, M.S., Routh, A.L., Ren, P., Ku, Z., An, Z., Debbink, K., Diamond, M.S., Shi, P.-Y., Freiberg, A.N., Menachery, V.D., 2021. Loss of furin cleavage site attenuates SARS-CoV-2 pathogenesis. Nature 591, 293–299. https://doi.org/10.1038/s41586-021-03237-4

Johnson, B.A., Zhou, Y., Lokugamage, K.G., Vu, M.N., Bopp, N., Crocquet-Valdes, P.A., Kalveram, B., Schindewolf, C., Liu, Y., Scharton, D., Plante, J.A., Xie, X., Aguilar, P., Weaver, S.C., Shi, P.-Y., Walker, D.H., Routh, A.L., Plante, K.S., Menachery, V.D., 2022. Nucleocapsid mutations in SARS-CoV-2 augment replication and pathogenesis. PLOS Pathogens 18, e1010627. https://doi.org/10.1371/journal.ppat.1010627

Kalyaanamoorthy, S., Minh, B.Q., Wong, T.K.F., von Haeseler, A., Jermiin, L.S., 2017. ModelFinder: fast model selection for accurate phylogenetic estimates. Nat Methods 14, 587–589. https://doi.org/10.1038/nmeth.4285

Kimura, I., Yamasoba, D., Nasser, H., Zahradnik, J., Kosugi, Y., Wu, J., Nagata, K., Uriu, K., Tanaka, Y.L., Ito, J., Shimizu, R., Tan, T.S., Butlertanaka, E.P., Asakura, H., Sadamasu, K., Yoshimura, K., Ueno, T., Takaori-Kondo, A., Schreiber, G., Genotype to Phenotype Japan (G2P-Japan) Consortium, Toyoda, M., Shirakawa, K., Irie, T., Saito, A., Nakagawa, S., Ikeda, T., Sato, K., 2022. The SARS-CoV-2 spike S375F mutation characterizes the Omicron BA.1 variant. iScience 25, 105720. https://doi.org/10.1016/j.isci.2022.105720

Lahti, D.C., Johnson, N.A., Ajie, B.C., Otto, S.P., Hendry, A.P., Blumstein, D.T., Coss, R.G., Donohue, K., Foster, S.A., 2009. Relaxed selection in the wild. Trends in Ecology & Evolution 24, 487–496. https://doi.org/10.1016/j.tree.2009.03.010

Lamers, M.M., Mykytyn, A.Z., Breugem, T.I., Groen, N., Knoops, K., Schipper, D., Acker, R. van, Doel, P.B. van den, Bestebroer, T., Koopman, C.D., Reusken, C., Muraro, M.J., GeurtsvanKessel, C.H., Royen, M.E. van, Peters, P.J., Zhang, J., Haagmans, B.L., 2022. SARS-CoV-2 Omicron efficiently infects human airway, but not alveolar epithelium. bioRxiv 2022.01.19.476898. https://doi.org/10.1101/2022.01.19.476898

Lauring, A.S., Andino, R., 2010. Quasispecies Theory and the Behavior of RNA Viruses. PLOS Pathogens 6, e1001005. https://doi.org/10.1371/journal.ppat.1001005

Lavine, J.S., Bjornstad, O.N., Antia, R., 2021. Immunological characteristics govern the transition of COVID-19 to endemicity. Science 371, 741–745. https://doi.org/10.1126/science.abe6522

Leung, K., Shum, M.H., Leung, G.M., Lam, T.T., Wu, J.T., 2021. Early transmissibility assessment of the N501Y mutant strains of SARS-CoV-2 in the United Kingdom, October to November 2020. Eurosurveillance 26, 2002106. https://doi.org/10.2807/1560-7917.ES.2020.26.1.2002106

Li, H., 2018. Minimap2: pairwise alignment for nucleotide sequences. Bioinformatics 34, 3094–3100. https://doi.org/10.1093/bioinformatics/bty191

Li, H., 2013. Aligning sequence reads, clone sequences and assembly contigs with BWA-MEM. arXiv.

Liu, Y., Liu, J., Plante, K.S., Plante, J.A., Xie, X., Zhang, X., Ku, Z., An, Z., Scharton, D., Schindewolf, C., Widen, S.G., Menachery, V.D., Shi, P.-Y., Weaver, S.C., 2022. The N501Y spike substitution enhances SARS-CoV-2 infection and transmission. Nature 602, 294–299. https://doi.org/10.1038/s41586-021-04245-0

Lythgoe, K., Golubchik, T., Hall, M., House, T., Cahuantzi, R., MacIntyre-Cockett, G., Fryer, H., Thomson, L., Nurtay, A., Ghafani, M., Buck, D., Green, A., Trebes, A., Piazza, P., Lonie, L.J., Studley, R., Rourke, E., Smith, D., Bashton, M., Nelson, A., Crown, M., McCann, C., Young, G.R., Santos, R.A.N. dos, Richards, Z., Tariq, A., Team, W.S.I.C.-19 S., Group, C.-19 I.S., Consortium, T.C.-19 G.U. (COG-U., Fraser, C., Diamond, I., Barrett, J., Walker, A.S., Bonsall, D., 2023. Lineage replacement and

evolution captured by three years of the United Kingdom Covid Infection Survey. https://doi.org/10.1101/2022.01.05.21268323
Markov, P.V., Ghafari, M., Beer, M., Lythgoe, K., Simmonds, P., Stilianakis, N.I., Katzourakis, A., 2023. The evolution of SARS-CoV-2. Nat Rev Microbiol 21, 361–379. https://doi.org/10.1038/s41579-023-00878-2
Minor, P.D., 2015. Live attenuated vaccines: Historical successes and current challenges. Virology, 60th Anniversary Issue 479–480, 379–392. https://doi.org/10.1016/j.virol.2015.03.032
Mölder, F., Jablonski, K.P., Letcher, B., Hall, M.B., Tomkins-Tinch, C.H., Sochat, V., Forster, J., Lee, S., Twardziok, S.O., Kanitz, A., Wilm, A., Holtgrewe, M., Rahmann, S., Nahnsen, S., Köster, J., 2021. Sustainable data analysis with Snakemake. F1000Res 10, 33. https://doi.org/10.12688/f1000research.29032.2
Moya, A., Holmes, E.C., González-Candelas, F., 2004. The population genetics and evolutionary epidemiology of RNA viruses. Nat Rev Microbiol 2, 279–288. https://doi.org/10.1038/nrmicro863
Nguyen, L.-T., Schmidt, H.A., von Haeseler, A., Minh, B.Q., 2015. IQ-TREE: A Fast and Effective Stochastic Algorithm for Estimating Maximum-Likelihood Phylogenies. Molecular Biology and Evolution 32, 268–274. https://doi.org/10.1093/molbev/msu300
Ogando, N.S., Dalebout, T.J., Zevenhoven-Dobbe, J.C., Limpens, R.W.A.L., van der Meer, Y., Caly, L., Druce, J., de Vries, J.J.C., Kikkert, M., Bárcena, M., Sidorov, I., Snijder, E.J., 2020. SARS-coronavirus-2 replication in Vero E6 cells: replication kinetics, rapid adaptation and cytopathology. J Gen Virol 101, 925–940. https://doi.org/10.1099/jgv.0.001453
O'Toole, Á., Scher, E., Underwood, A., Jackson, B., Hill, V., McCrone, J.T., Colquhoun, R., Ruis, C., Abu-Dahab, K., Taylor, B., Yeats, C., Du Plessis, L., Maloney, D., Medd, N., Attwood, S.W., Aanensen, D.M., Holmes, E.C., Pybus, O.G., Rambaut, A., 2021. Assignment of Epidemiological Lineages in an Emerging Pandemic Using the Pangolin Tool. Virus Evolution. https://doi.org/10.1093/ve/veab064
Pedersen, B.S., Quinlan, A.R., 2017. cyvcf2: fast, flexible variant analysis with Python. Bioinformatics 33, 1867–1869. https://doi.org/10.1093/bioinformatics/btx057
Quinlan, A.R., Hall, I.M., 2010. BEDTools: a flexible suite of utilities for comparing genomic features. Bioinformatics 26, 841–842. https://doi.org/10.1093/bioinformatics/btq033
Redondo, N., Zaldívar-López, S., Garrido, J.J., Montoya, M., 2021. SARS-CoV-2 Accessory Proteins in Viral Pathogenesis: Knowns and Unknowns. Frontiers in Immunology 12.
Saito, A., Irie, T., Suzuki, R., Maemura, T., Nasser, H., Uriu, K., Kosugi, Y., Shirakawa, K., Sadamasu, K., Kimura, I., Ito, J., Wu, J., Iwatsuki-Horimoto, K., Ito, M., Yamayoshi, S., Loeber, S., Tsuda, M., Wang, L., Ozono, S., Butlertanaka, E.P., Tanaka, Y.L., Shimizu, R., Shimizu, K., Yoshimatsu, K., Kawabata, R., Sakaguchi, T., Tokunaga, K., Yoshida, I., Asakura, H., Nagashima, M., Kazuma, Y., Nomura, R., Horisawa, Y., Yoshimura, K., Takaori-Kondo, A., Imai, M., Tanaka, S., Nakagawa, S., Ikeda, T., Fukuhara, T., Kawaoka, Y., Sato, K., 2022. Enhanced fusogenicity and pathogenicity of SARS-CoV-2 Delta P681R mutation. Nature 602, 300–306. https://doi.org/10.1038/s41586-021-04266-9
Sasaki, M., Uemura, K., Sato, A., Toba, S., Sanaki, T., Maenaka, K., Hall, W.W., Orba, Y., Sawa, H., 2021. SARS-CoV-2 variants with mutations at the S1/S2 cleavage site are generated in vitro during propagation in TMPRSS2-deficient cells. PLOS Pathogens 17, e1009233. https://doi.org/10.1371/journal.ppat.1009233
Shuai, L., Zhong, G., Yuan, Q., Wen, Z., Wang, C., He, X., Liu, R., Wang, J., Zhao, Q., Liu, Y., Huo, N., Deng, J., Bai, J., Wu, H., Guan, Y., Shi, J., Tian, K., Xia, N., Chen, H.,

Bu, Z., 2020. Replication, pathogenicity, and transmission of SARS-CoV-2 in minks. Natl Sci Rev 8, nwaa291. https://doi.org/10.1093/nsr/nwaa291

Takada, K., Ueda, M.T., Shichinohe, S., Kida, Y., Ono, C., Matsuura, Y., Watanabe, T., Nakagawa, S., 2023. Genomic diversity of SARS-CoV-2 can be accelerated by mutations in the nsp14 gene. iScience 26, 106210. https://doi.org/10.1016/j.isci.2023.106210

Tay, J.H., Porter, A.F., Wirth, W., Duchene, S., 2022. The Emergence of SARS-CoV-2 Variants of Concern Is Driven by Acceleration of the Substitution Rate. Molecular Biology and Evolution 39, msac013. https://doi.org/10.1093/molbev/msac013

Viana, R., Moyo, S., Amoako, D.G., Tegally, H., Scheepers, C., Althaus, C.L., Anyaneji, U.J., Bester, P.A., Boni, M.F., Chand, M., Choga, W.T., Colquhoun, R., Davids, M., Deforche, K., Doolabh, D., du Plessis, L., Engelbrecht, S., Everatt, J., Giandhari, J., Giovanetti, M., Hardie, D., Hill, V., Hsiao, N.-Y., Iranzadeh, A., Ismail, A., Joseph, C., Joseph, R., Koopile, L., Kosakovsky Pond, S.L., Kraemer, M.U.G., Kuate-Lere, L., Laguda-Akingba, O., Lesetedi-Mafoko, O., Lessells, R.J., Lockman, S., Lucaci, A.G., Maharaj, A., Mahlangu, B., Maponga, T., Mahlakwane, K., Makatini, Z., Marais, G., Maruapula, D., Masupu, K., Matshaba, M., Mayaphi, S., Mbhele, N., Mbulawa, M.B., Mendes, A., Mlisana, K., Mnguni, A., Mohale, T., Moir, M., Moruisi, K., Mosepele, M., Motsatsi, G., Motswaledi, M.S., Mphoyakgosi, T., Msomi, N., Mwangi, P.N., Naidoo, Y., Ntuli, N., Nyaga, M., Olubayo, L., Pillay, S., Radibe, B., Ramphal, Y., Ramphal, U., San, J.E., Scott, L., Shapiro, R., Singh, L., Smith-Lawrence, P., Stevens, W., Strydom, A., Subramoney, K., Tebeila, N., Tshiabuila, D., Tsui, J., van Wyk, S., Weaver, S., Wibmer, C.K., Wilkinson, E., Wolter, N., Zarebski, A.E., Zuze, B., Goedhals, D., Preiser, W., Treurnicht, F., Venter, M., Williamson, C., Pybus, O.G., Bhiman, J., Glass, A., Martin, D.P., Rambaut, A., Gaseitsiwe, S., von Gottberg, A., de Oliveira, T., 2022. Rapid epidemic expansion of the SARS-CoV-2 Omicron variant in southern Africa. Nature 603, 679–686. https://doi.org/10.1038/s41586-022-04411-y

Weigang, S., Fuchs, J., Zimmer, G., Schnepf, D., Kern, L., Beer, J., Luxenburger, H., Ankerhold, J., Falcone, V., Kemming, J., Hofmann, M., Thimme, R., Neumann-Haefelin, C., Ulferts, S., Grosse, R., Hornuss, D., Tanriver, Y., Rieg, S., Wagner, D., Huzly, D., Schwemmle, M., Panning, M., Kochs, G., 2021. Within-host evolution of SARS-CoV-2 in an immunosuppressed COVID-19 patient as a source of immune escape variants. Nat Commun 12, 6405. https://doi.org/10.1038/s41467-021-26602-3

Wilm, A., Aw, P.P.K., Bertrand, D., Yeo, G.H.T., Ong, S.H., Wong, C.H., Khor, C.C., Petric, R., Hibberd, M.L., Nagarajan, N., 2012. LoFreq: a sequence-quality aware, ultra-sensitive variant caller for uncovering cell-population heterogeneity from high-throughput sequencing datasets. Nucleic Acids Res 40, 11189–11201. https://doi.org/10.1093/nar/gks918

Yamamoto, M., Tomita, K., Hirayama, Y., Inoue, J., Kawaguchi, Y., Gohda, J., 2022. SARS-CoV-2 Omicron spike H655Y mutation is responsible for enhancement of the endosomal entry pathway and reduction of cell surface entry pathways. https://doi.org/10.1101/2022.03.21.485084

Yuan, M., Chen, X., Zhu, Y., Dong, X., Liu, Y., Qian, Z., Ye, L., Liu, P., 2022. A Bispecific Antibody Targeting RBD and S2 Potently Neutralizes SARS-CoV-2 Omicron and Other Variants of Concern. Journal of Virology 96. https://doi.org/10.1128/jvi.00775-22

Yurkovetskiy, L., Wang, X., Pascal, K.E., Tomkins-Tinch, C., Nyalile, T.P., Wang, Y., Baum, A., Diehl, W.E., Dauphin, A., Carbone, C., Veinotte, K., Egri, S.B., Schaffner, S.F., Lemieux, J.E., Munro, J.B., Rafique, A., Barve, A., Sabeti, P.C., Kyratsous, C.A., Dudkina, N.V., Shen, K., Luban, J., 2020. Structural and Functional Analysis of the

D614G SARS-CoV-2 Spike Protein Variant. Cell 183, 739-751.e8. https://doi.org/10.1016/j.cell.2020.09.032

Zandi, M., Shafaati, M., Kalantar-Neyestanaki, D., Pourghadamyari, H., Fani, M., Soltani, S., Kaleji, H., Abbasi, S., 2022. The role of SARS-CoV-2 accessory proteins in immune evasion. Biomedicine & Pharmacotherapy 156, 113889. https://doi.org/10.1016/j.biopha.2022.113889

Zhou, B., Thao, T.T.N., Hoffmann, D., Taddeo, A., Ebert, N., Labroussaa, F., Pohlmann, A., King, J., Steiner, S., Kelly, J.N., Portmann, J., Halwe, N.J., Ulrich, L., Trüeb, B.S., Fan, X., Hoffmann, B., Wang, L., Thomann, L., Lin, X., Stalder, H., Pozzi, B., de Brot, S., Jiang, N., Cui, D., Hossain, J., Wilson, M.M., Keller, M.W., Stark, T.J., Barnes, J.R., Dijkman, R., Jores, J., Benarafa, C., Wentworth, D.E., Thiel, V., Beer, M., 2021. SARS-CoV-2 spike D614G change enhances replication and transmission. Nature 592, 122–127. https://doi.org/10.1038/s41586-021-03361-1

Zinzula, L., 2021. Lost in deletion: The enigmatic ORF8 protein of SARS-CoV-2. Biochemical and Biophysical Research Communications, COVID-19 538, 116–124. https://doi.org/10.1016/j.bbrc.2020.10.045

Figures

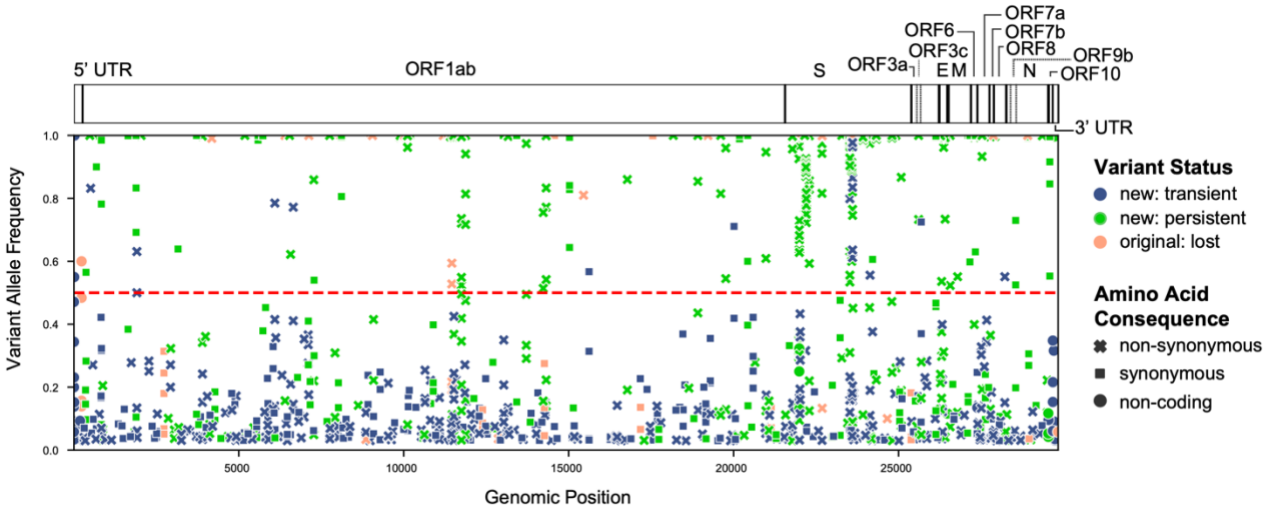

Figure 1: The location of all detected variants across all samples in all passage lines. The colour of points indicates whether a variant was present in the original clinical isolate ('original: lost'), or arose new during serial passaging but was then lost ('new: transient') or persisted in the final passage number ('new: persistent'). The shape of points corresponds to the inferred amino acid consequence, either non-synonymous, synonymous, or 'other' (in non-coding regions). All points above the horizontal dashed line are the majority allele for a given sample (allele frequency ≥50%). The location of genes within the SARS-CoV-2 genome is indicated above the plot in a schematic of the complete SARS CoV-2 genome of ~30 kb.

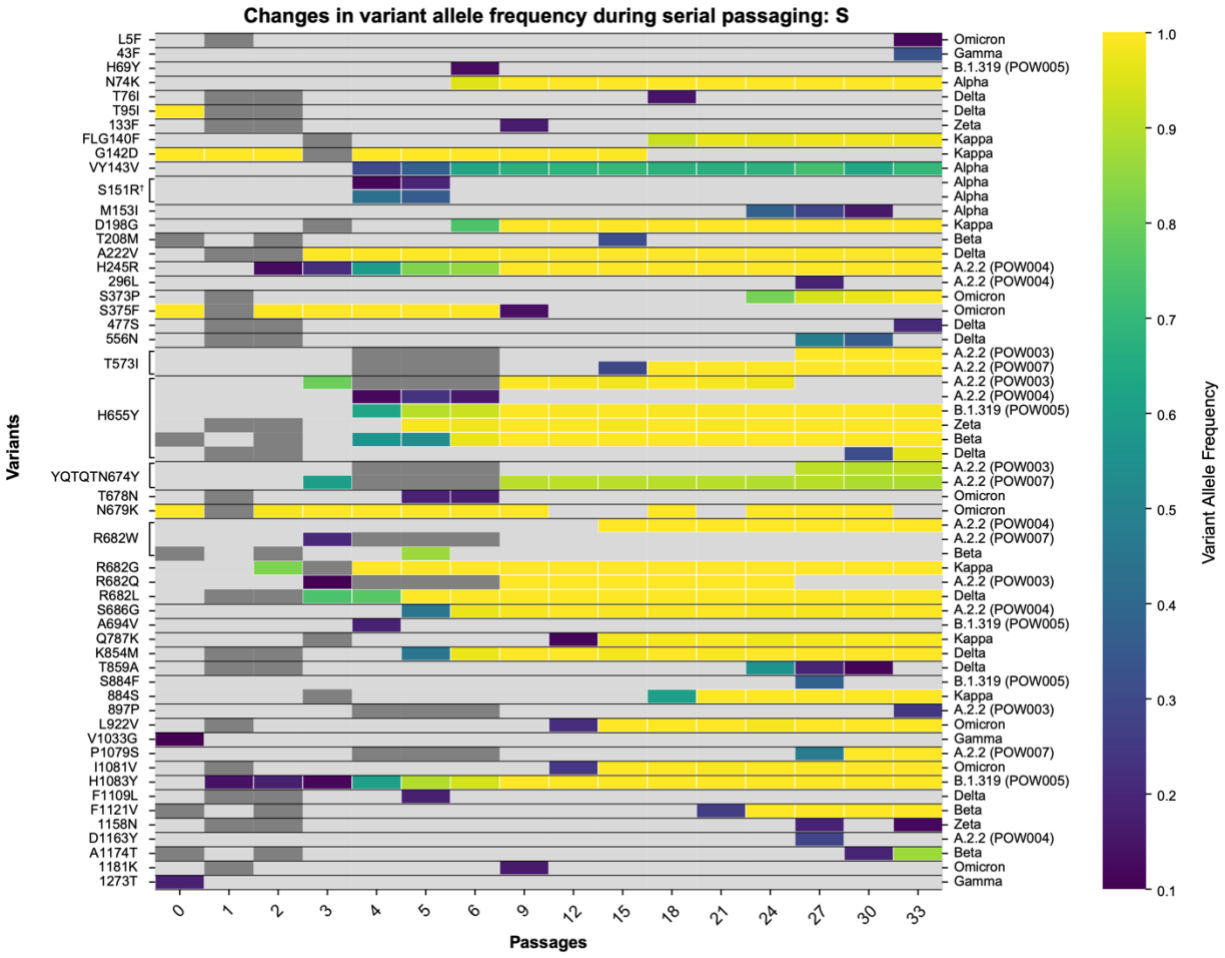

Figure 2: Heatmap depicting the variants detected in the spike gene of SARS-CoV-2 in each passage line throughout the course of serial passaging. The x-axis refers to the passage number (range: 0 [clinical isolate] to 33). On the primary y-axis (lefthand side) the inferred amino acid changes of variants are listed (see Supplementary Table S1 for further detail). On the secondary y-axis (righthand side) the data in a given row is linked to the passage line from which it derives. Each 'cell' within the heatmap is shaded based on the variant allele frequency of a given variant in a given passage number within that passage line (light grey: undetected). Any cells that are dark grey represent cases where there is no sequencing data for that passage number. Convergence among passage lines is indicated by brackets linking a given variant to multiple passage lines.

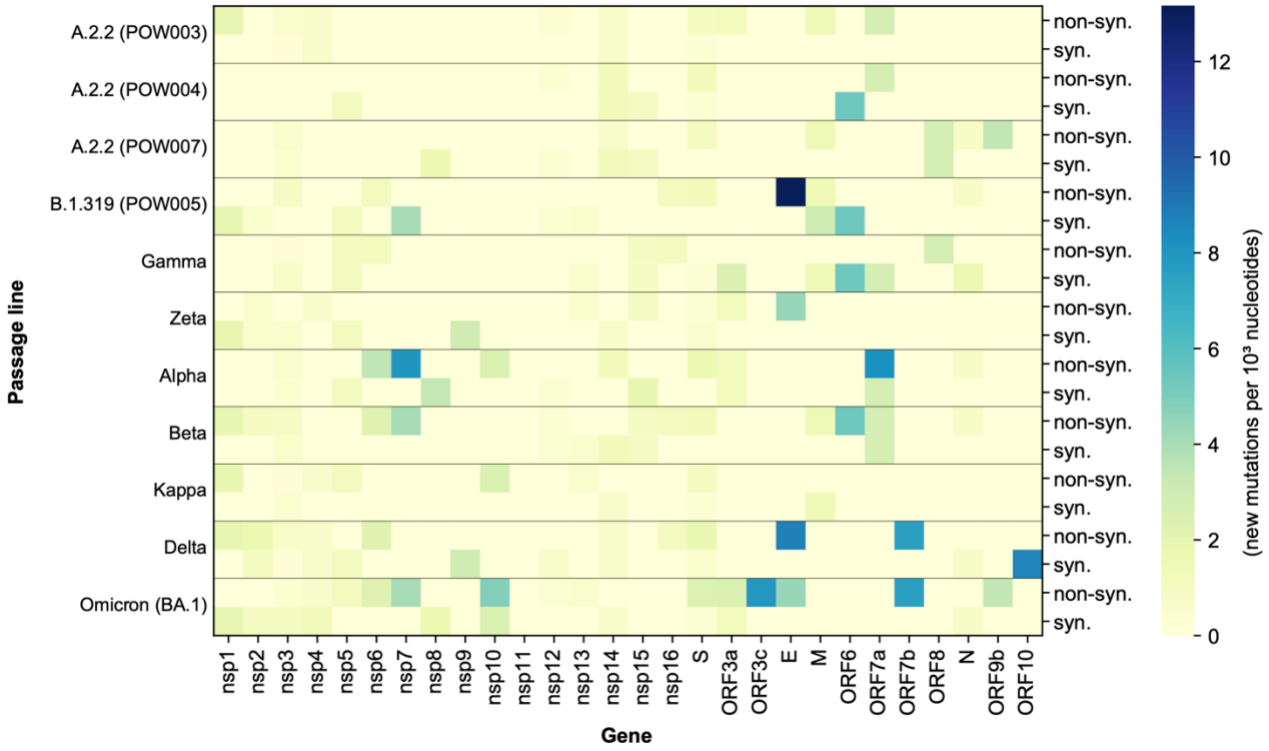

Figure 3: Heatmap depicting the number of total number of new mutations within each gene of the SARS-CoV-2 genome (normalised by gene length) throughout a maximum of 33 serial passages, highlighting the trends within different passage lines.

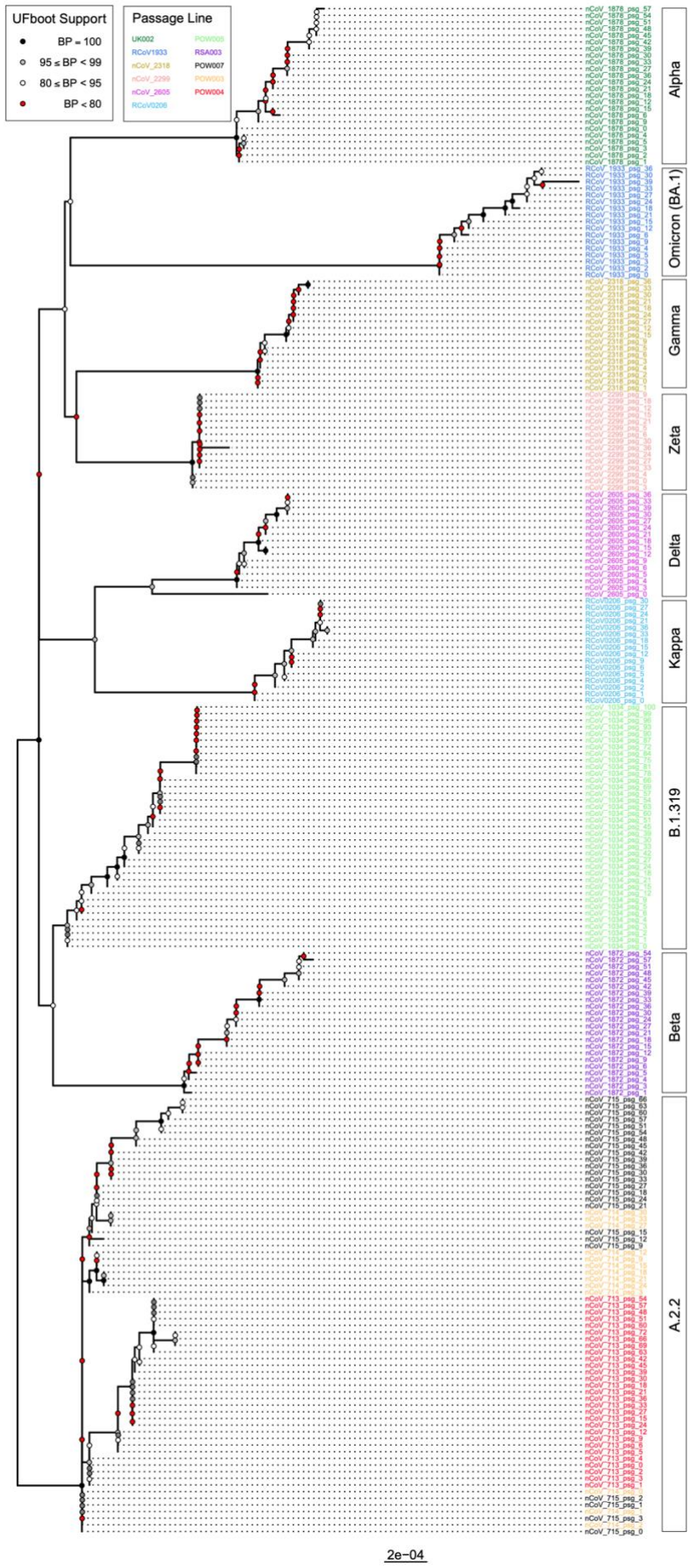
UFboot Support
BP = 100
95 ≤ BP < 99
80 ≤ BP < 95
BP < 80
Passage Line
UK002
POW005
RCoV1933
RSA003
nCoV_2318
POW007
nCoV_2299
POW003
nCoV_2605
POW004
RCoV0206
Alpha
Omicron (BA.1)
Gamma
Zeta
Delta
Kappa
B.1.319
Beta
A.2.2
2e−04

Figure 4: Phylogenetic tree depicting the inferred phylogenetic relationships among all samples in the study. The support for relationships (ultrafast bootstrap support, “UFboot”) is represented by shaded circles at nodes. Tip labels are shaded to reflect passage lines. The lineage calls for samples are depicted in rectangles to the right of the tree.

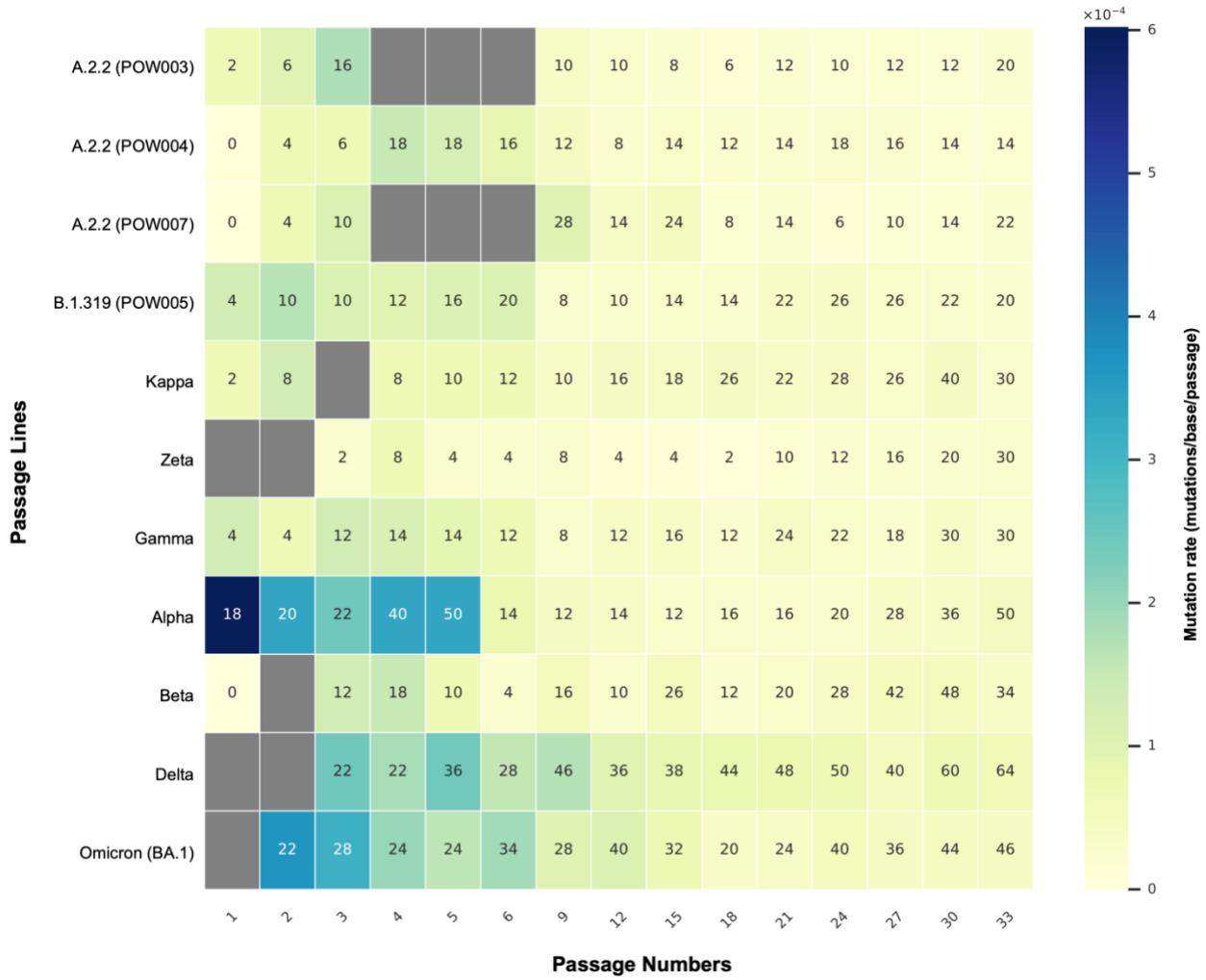

Figure 5: Heatmap depicting the inferred mutation rate (mutations per base per passage) at each passage number within each passage line. The rate was calculated based on the number of de novo mutations detected in a given passage number relative to the previous passage number (see main text). Each ‘cell’ in the heatmap is shaded based on the inferred mutation rate, and numbers within the cell represent the total number of variants called in that sample relative to the Wuhan Hu-1 reference genome for SARS-CoV-2. The purging of mutations (often those at a low variant allele frequency) during serial passaging can be observed, for example when comparing passages 5 and in the Alpha passage line.

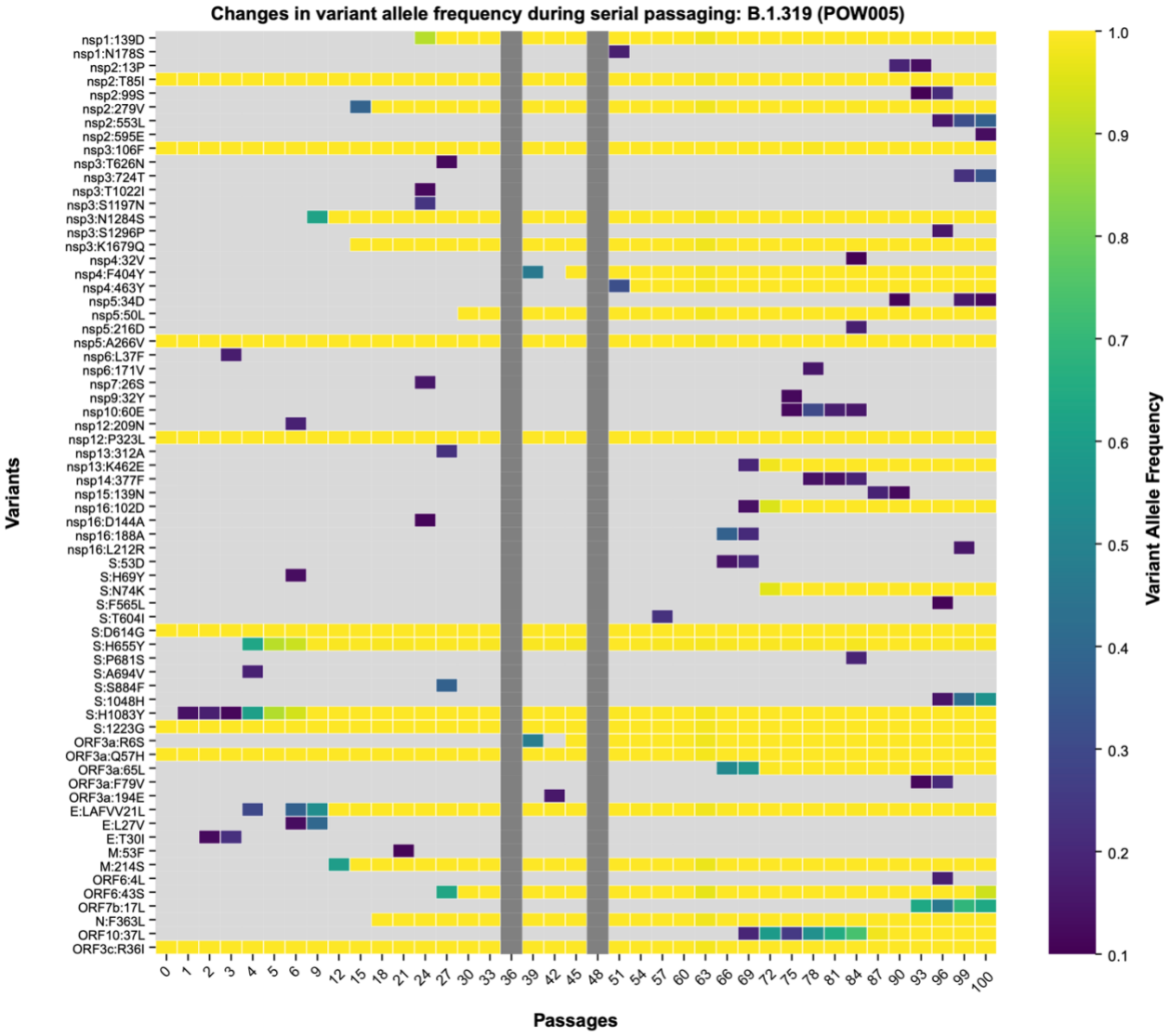

Figure 6: Heatmap depicting the variants detected in the each gene of SARS-CoV-2 in the POW005 passage line throughout the course of 100 serial passages. The x-axis refers to the passage number (range: 0 [clinical isolate] to 100). On the y-axis the inferred amino acid changes of variants in each gene are listed (see Supplementary Table S1 for further detail). Each 'cell' within the heatmap is shaded based on the variant allele frequency of a given variant in a given passage number within that passage line (light grey: undetected). Any cells that are dark grey represent cases where there is no sequencing data for that passage number.

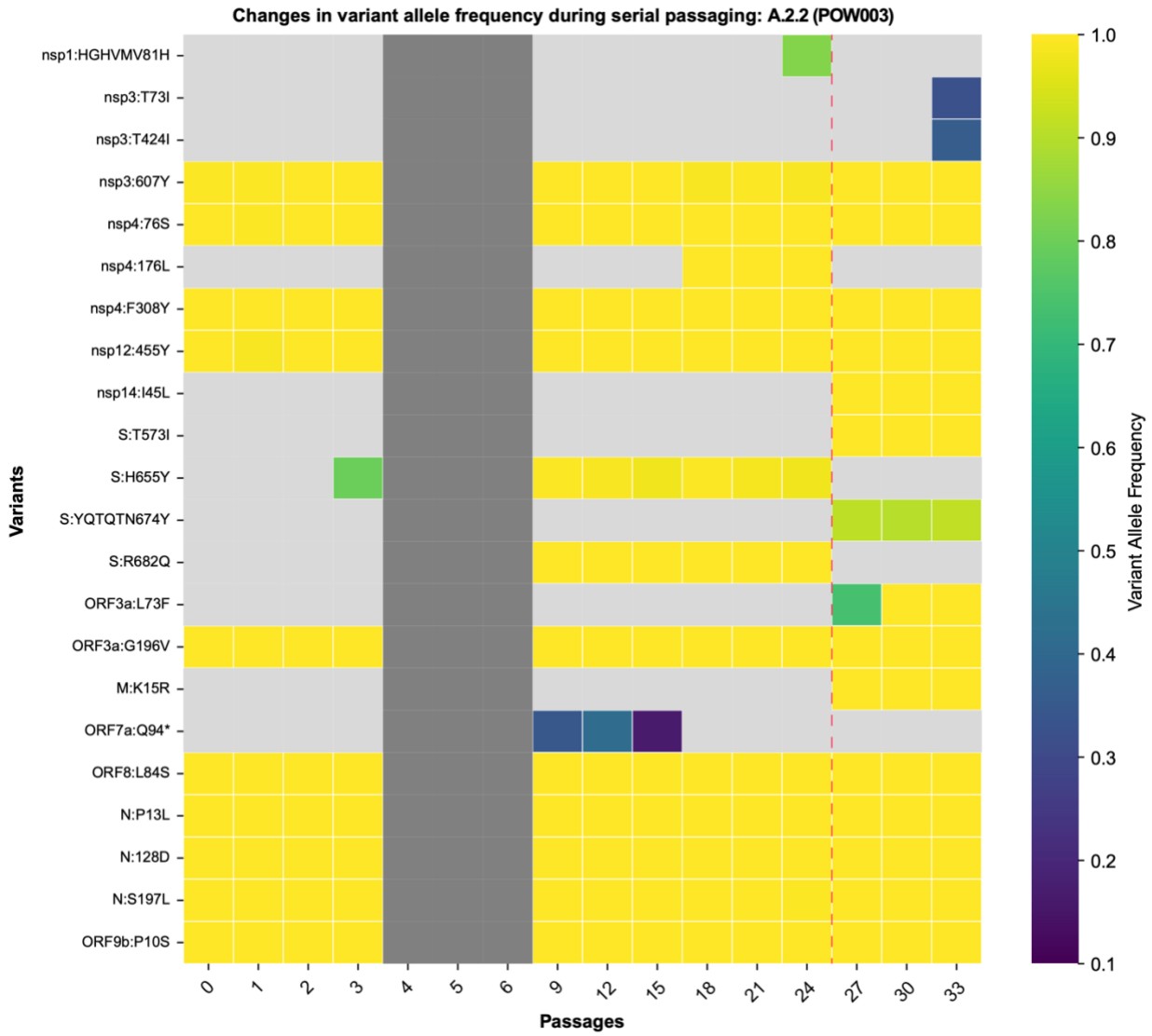

Figure 7: Heatmap depicting the variants detected in the each gene of SARS-CoV-2 in the POW003 passage line throughout the course of 33 serial passages. The x-axis refers to the passage number (range: 0 [clinical isolate] to 33). On the y-axis the inferred amino acid changes of variants in each gene are listed (see Supplementary Table S1 for further detail). Each 'cell' within the heatmap is shaded based on the variant allele frequency of a given variant in a given passage number within that passage line (light grey: undetected). Any cells that are dark grey represent cases where there is no sequencing data for that passage number. The vertical dashed line represents a boundary point at which a partial haplotype replacement is inferred to have occurred (between passages 24 and 27) given the abrupt appearance of several fixed/high-frequency variants.

Tables

Table 1: Overview of the passage lines used within this study, including their nomenclatural assignments and the number of serial passages

Sample ID	GISAID Accession†	Pango Lineage	WHO Name*	Maximum Passage Number
POW003	EPI_ISL_707892	A.2.2	–	33
POW004	EPI_ISL_8767166	A.2.2	–	72
POW007	EPI_ISL_678338	A.2.2	–	66
POW005	EPI_ISL_18218201	B.1.319	–	100
nCoV_2318	EPI_ISL_1121976	P.1	Gamma	36
nCoV_2299	EPI_ISL_18218200	P.2	Zeta	36
UK002	EPI_ISL_794671	B.1.1.7	Alpha	57
RSA003	EPI_ISL_775245	B.1.351	Beta	57
RCoV0206	EPI_ISL_1660480	B.1.617.1	Kappa	39
nCoV_2605	EPI_ISL_1911187	B.1.617.2	Delta	39
RCoV1933	EPI_ISL_6814922	BA.1	Omicron (BA.1)	39

† All accessions here refer to consensus genomes from passage 0 (or the earliest available passage) that were uploaded to GISAID

* Names assigned by the World Health Organisation for Variants of Concern or Variants Under Investigation

Table 2: All variants that arose *de novo* during the course of *in vitro* serial passaging that were also present (either originally or newly arising) in at least one other passage lines. The numbers in square brackets in the 'lines' column refer to the maximum variant allele frequency that each variant was detected at in each corresponding passage line.

Variant	**Gene**	**Amino Acid Change**	**Effect**	**Passage Lines**
T2C	5' UTR	None	None	A.2.2 (POW003) [new: 0.231], A.2.2 (POW007) [new: 0.344], B.1.319 (POW005) [new: 0.471]
C6402T	nsp3	P1228L	missense	Alpha [new: 0.157], Delta [original: 1]
T11522G	nsp6	F184V	missense	Alpha [new: 0.425], Omicron (BA.1) [new: 0.1]
C11750T	nsp6	L260F	missense	Gamma [new: 1], Alpha [new: 1], Beta [new: 1]
C13860T	nsp12	140D	synonymous	Gamma [original: 1], Beta [new: 0.117]
ATACATG21764A	S	IHV68I	inframe deletion	Alpha [original: 1], Omicron (BA.1) [new: 1]

C23280T	S	T573I	missense	A.2.2 (POW003) [new: 1], A.2.2 (POW007) [new: 1]
C23525T	S	H655Y	missense	A.2.2 (POW003) [new: 0.994], A.2.2 (POW004) [new: 0.233], B.1.319 (POW005) [new: 0.996], Gamma [original: 1], Zeta [new: 1], Beta [new: 1], Delta [new: 0.964], Omicron (BA.1) [original: 1]
TATCAGACTCAGACTA23582T	S	YQTQTN674Y	inframe deletion	A.2.2 (POW003) [new: 0.914], A.2.2 (POW007) [new: 0.912]
C23606T	S	R682W	missense	A.2.2 (POW004) [new: 1], A.2.2 (POW007) [new: 0.204], Alpha [new: 0.977], Beta [new: 0.865]
C26270T	E	T9I	missense	Zeta [new: 0.241], Omicron (BA.1) [original: 1]
A26566G	M	K15R	missense	A.2.2 (POW003) [new: 1], A.2.2 (POW007) [new: 1]
C26681T	M	53F	synonymous	B.1.319 (POW005) [new: 0.108], Kappa [original: 1]

Table 3: All mutations arising *de novo* throughout the course of long-term serial passaging that are noted in a compendium of functional impacts of mutations in the SARS-CoV-2 Wuhan Hu-1 reference genome (https://github.com/nodrogluap/pokay). All passage lines we studied (see text) are noted in the first column. Reference numbers refer to those in Supplementary File S1.

Passage Line	Gene	Amino Acid Consequences	Category	Reference(s)
Kappa	nsp5	T21I	pharmaceutical effectiveness	1; 2
B.1.319 (POW005)	nsp6	L37F	homoplasy	3; 4; 5; 6; 7
Omicron	S	L5F	ACE2 receptor binding affinity	8; 9
			convalescent plasma binding	8; 9; 10; 11; 12
			vaccine efficacy	13; 14
			vaccine neutralization efficacy	8; 9; 10; 12; 15; 16; 17
			vaccinee plasma binding	8; 9
Gamma	S	43F	monoclonal antibody serial passage escape	18
			pharmaceutical effectiveness	19; 20

Omicron	S	A67V	ACE2 receptor binding affinity	21; 22
			antibody epitope effects	23; 24; 25; 26; 27
			pharmaceutical effectiveness	28; 29; 30; 31
			vaccine neutralization efficacy	16; 17; 21; 22; 28; 29; 30; 32; 33; 34; 35
			vaccinee plasma binding	32; 35; 36
Alpha	S	N74K	homoplasy	37; 38
Delta	S	T76I	convalescent plasma escape	39; 40
			pharmaceutical effectiveness	41
			vaccine neutralization efficacy	39; 40
Delta	S	A222V	antibody epitope effects	42; 43
			convalescent plasma escape	44; 45
			humoral response durability	46
			reinfection	46
			vaccine neutralization efficacy	44; 45
Omicron	S	S373P	ACE2 receptor binding affinity	21; 22; 47; 48
			antibody epitope effects	23; 24; 25; 26; 27
			monoclonal antibody serial passage escape	49
			pharmaceutical effectiveness	28; 29; 30
			transmissibility	50
			vaccine neutralization efficacy	21; 22; 30; 32; 33; 34; 35
			vaccinee plasma binding	32; 35; 36
A.2.2 (POW003), A.2.2 (POW004), B.1.319 (POW005), Zeta, Beta, Delta	S	H655Y	ACE2 receptor binding affinity	8; 9; 21; 22
			T cell evasion	51; 52
			anthropozoonotic events	53; 54; 55; 56
			antibody epitope effects	23; 24; 25; 26; 27; 57; 58; 59
			convalescent plasma binding	8; 9; 60; 61; 62
			convalescent plasma escape	39; 40; 57; 58; 59; 63
			homoplasy	37; 38
			outcome hazard ratio	64; 65; 66
			pharmaceutical effectiveness	28; 29; 30; 31; 61; 67
			reinfection	68; 69
			trafficking	53; 61
			transmissibility	70; 71

			vaccine efficacy	13; 14
			vaccine neutralization efficacy	8; 9; 11; 15; 16; 17; 21; 22; 28; 29; 30; 32; 33; 34; 35; 39; 40; 51; 52; 57; 58; 59; 60; 61; 67; 72; 73; 74; 75; 76; 77; 78; 79
			vaccinee plasma binding	8; 9; 32; 35; 36
			virion structure	58; 59; 80
A.2.2 (POW004), A.2.2 (POW007), Alpha, Beta	S	R682W	anthropozoonotic events	53
			vaccine neutralization efficacy	77; 78; 81; 82; 83; 84; 85
A.2.2 (POW004)	S	S686G	anthropozoonotic events	86
Zeta	E	T9I	frequency based fitness	87
			homoplasy	37; 38
B.1.319 (POW005)	E	T30I	homoplasy	37; 38
Kappa	M	41N	frequency based fitness	87
B.1.319 (POW005)	M	53F	frequency based fitness	87

Table 4: All mutations arising *de novo* throughout the course of long-term serial passaging that fall within nsp5, nsp10, nsp12, and nsp14 of the SARS-CoV-2 genome.

Passage Line	Gene	Amino Acid Consequence	Minimum VAF	Maximum VAF	First Appearance	Last Appearance
Kappa	nsp5	T21I	0.962	1	4	33
Omicron	nsp5	T198A	0.152	0.254	3	6
Gamma	nsp5	P252L	0.222	0.222	3	3
Alpha	nsp10	N3K	0.116	0.35	2	4
Omicron	nsp10	T47I	0.135	0.135	4	4
Kappa	nsp10	H48R	0.997	1	15	33
Omicron	nsp10	T49I	0.123	0.123	12	12
Beta	nsp12	D92A	0.291	0.974	24	33
Omicron	nsp12	P264S	0.156	0.755	27	33
A.2.2 (POW003)	nsp12	L280S	0.111	0.151	1	3
A.2.2 (POW004)	nsp12	T293I	0.14	1	2	33

A.2.2 (POW003)	nsp14	I45L	1	1	27	33
A.2.2 (POW007)	nsp14	P203L	0.197	0.197	33	33
A.2.2 (POW004)	nsp14	T293A	0.436	1	5	33
Delta	nsp14	P297S	0.127	0.127	18	18
A.2.2 (POW004)	nsp14	H424R	0.115	0.115	5	5
Alpha	nsp14	A504V	0.122	0.122	33	33
Alpha	nsp14	T524I	0.111	1	9	33

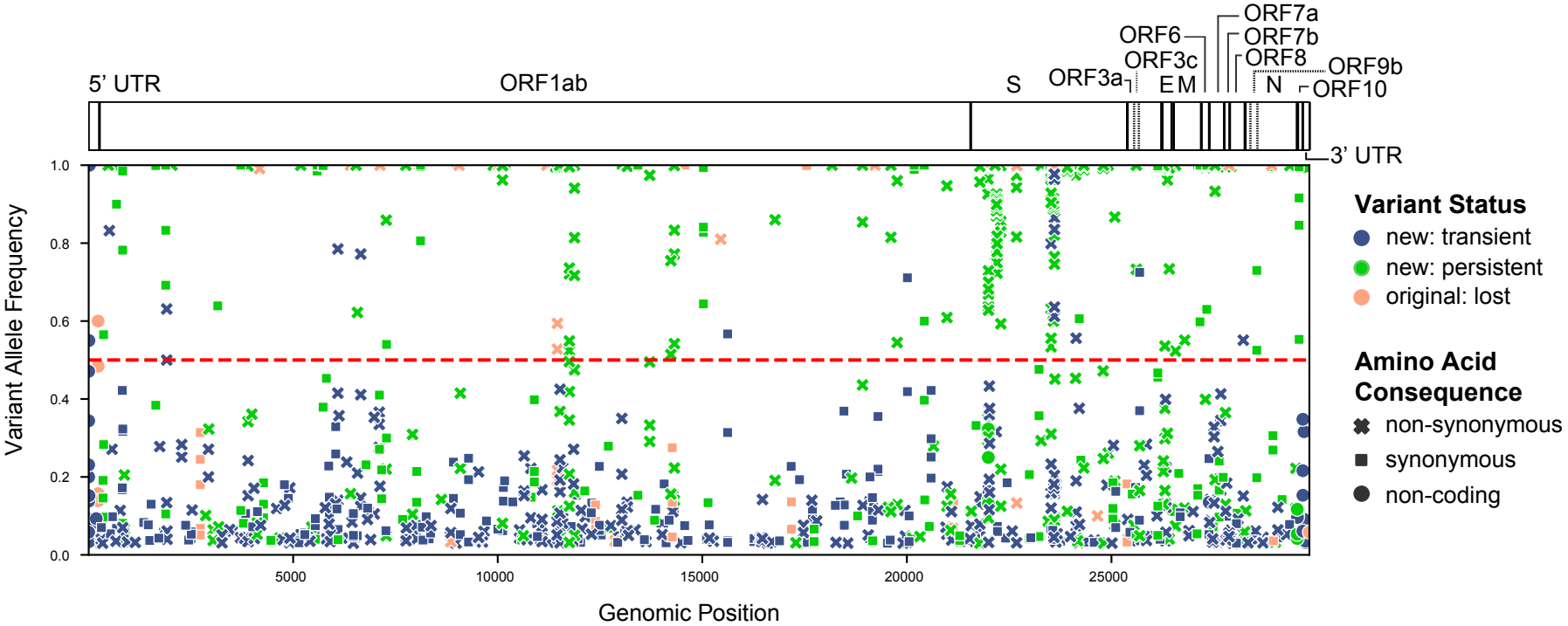
5' UTR
ORF1ab
S
ORF3a
ORF6
ORF3c
E
M
ORF7a
ORF7b
ORF8
N
ORF9b
ORF10
3' UTR
Variant Allele Frequency
1.0
0.8
0.6
0.4
0.2
0.0
5000
10000
15000
20000
25000
Genomic Position
Variant Status
new: transient
new: persistent
original: lost
Amino Acid Consequence
non-synonymous
synonymous
non-coding

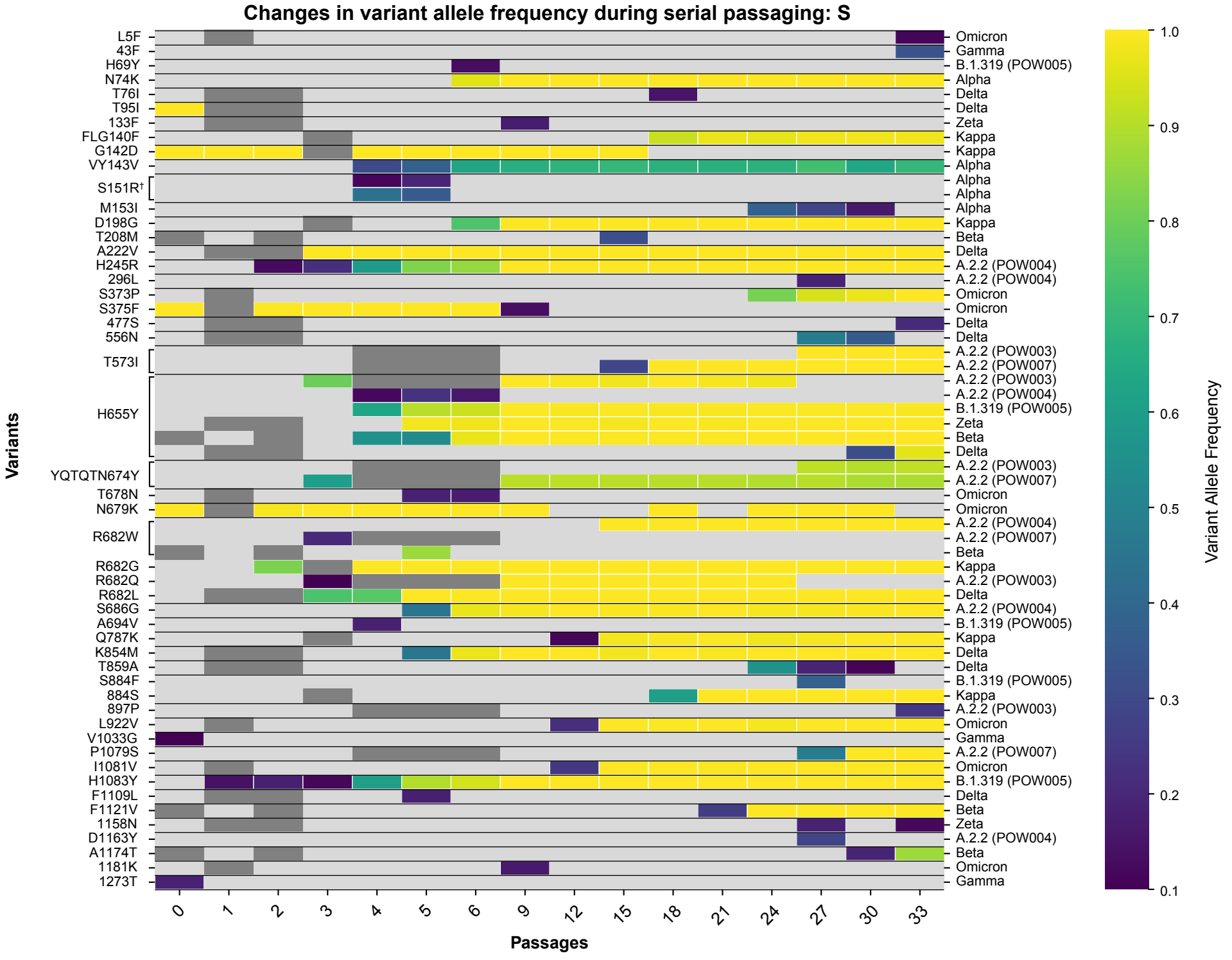
Changes in variant allele frequency during serial passaging: S
Variants
L5F
43F
H69Y
N74K
T76I
T95I
133F
FLG140F
G142D
VY143V
S151R†
M153I
D198G
T208M
A222V
H245R
296L
S373P
S375F
477S
556N
T573I
H655Y
YQTQTN674Y
T678N
N679K
R682W
R682G
R682Q
R682L
S686G
A694V
Q787K
K854M
T859A
S884F
884S
897P
L922V
V1033G
P1079S
I1081V
H1083Y
F1109L
F1121V
1158N
D1163Y
A1174T
1181K
1273T
Omicron
Gamma
B.1.319 (POW005)
Alpha
Delta
Delta
Zeta
Kappa
Kappa
Alpha
Alpha
Alpha
Alpha
Kappa
Beta
Delta
A.2.2 (POW004)
A.2.2 (POW004)
Omicron
Omicron
Delta
Delta
A.2.2 (POW003)
A.2.2 (POW007)
A.2.2 (POW003)
A.2.2 (POW004)
B.1.319 (POW005)
Zeta
Beta
Delta
A.2.2 (POW003)
A.2.2 (POW007)
Omicron
Omicron
A.2.2 (POW004)
A.2.2 (POW007)
Beta
Kappa
A.2.2 (POW003)
Delta
A.2.2 (POW004)
B.1.319 (POW005)
Kappa
Delta
Delta
B.1.319 (POW005)
Kappa
A.2.2 (POW003)
Omicron
Gamma
A.2.2 (POW007)
Omicron
B.1.319 (POW005)
Delta
Beta
Zeta
A.2.2 (POW004)
Beta
Omicron
Gamma
0
1
2
3
4
5
6
9
12
15
18
21
24
27
30
33
Passages
Variant Allele Frequency
1.0
0.9
0.8
0.7
0.6
0.5
0.4
0.3
0.2
0.1

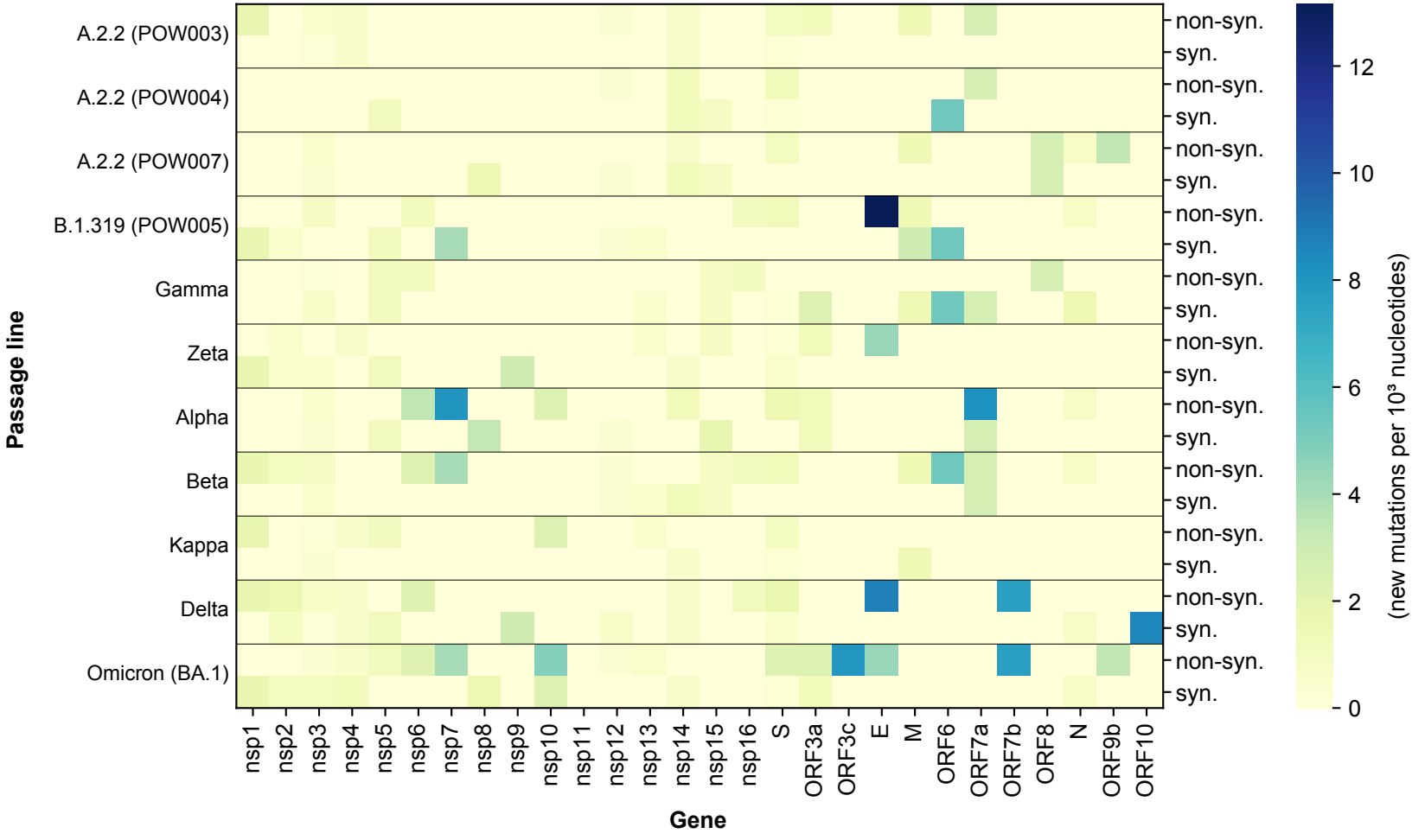
Passage line
A.2.2 (POW003)
A.2.2 (POW004)
A.2.2 (POW007)
B.1.319 (POW005)
Gamma
Zeta
Alpha
Beta
Kappa
Delta
Omicron (BA.1)
non-syn.
syn.
nsp1
nsp2
nsp3
nsp4
nsp5
nsp6
nsp7
nsp8
nsp9
nsp10
nsp11
nsp12
nsp13
nsp14
nsp15
nsp16
S
ORF3a
ORF3c
E
M
ORF6
ORF7a
ORF7b
ORF8
N
ORF9b
ORF10
Gene
0
2
4
6
8
10
12
(new mutations per 10³ nucleotides)

UFboot Support
BP = 100
95 ≤ BP < 99
80 ≤ BP < 95
BP < 80
Passage Line
UK002
RCoV1933
nCoV_2318
nCoV_2299
nCoV_2605
RCoV0206
POW005
RSA003
POW007
POW003
POW004
Alpha
Omicron (BA.1)
Gamma
Zeta
Delta
Kappa
B.1.319
Beta
A.2.2
2e−04

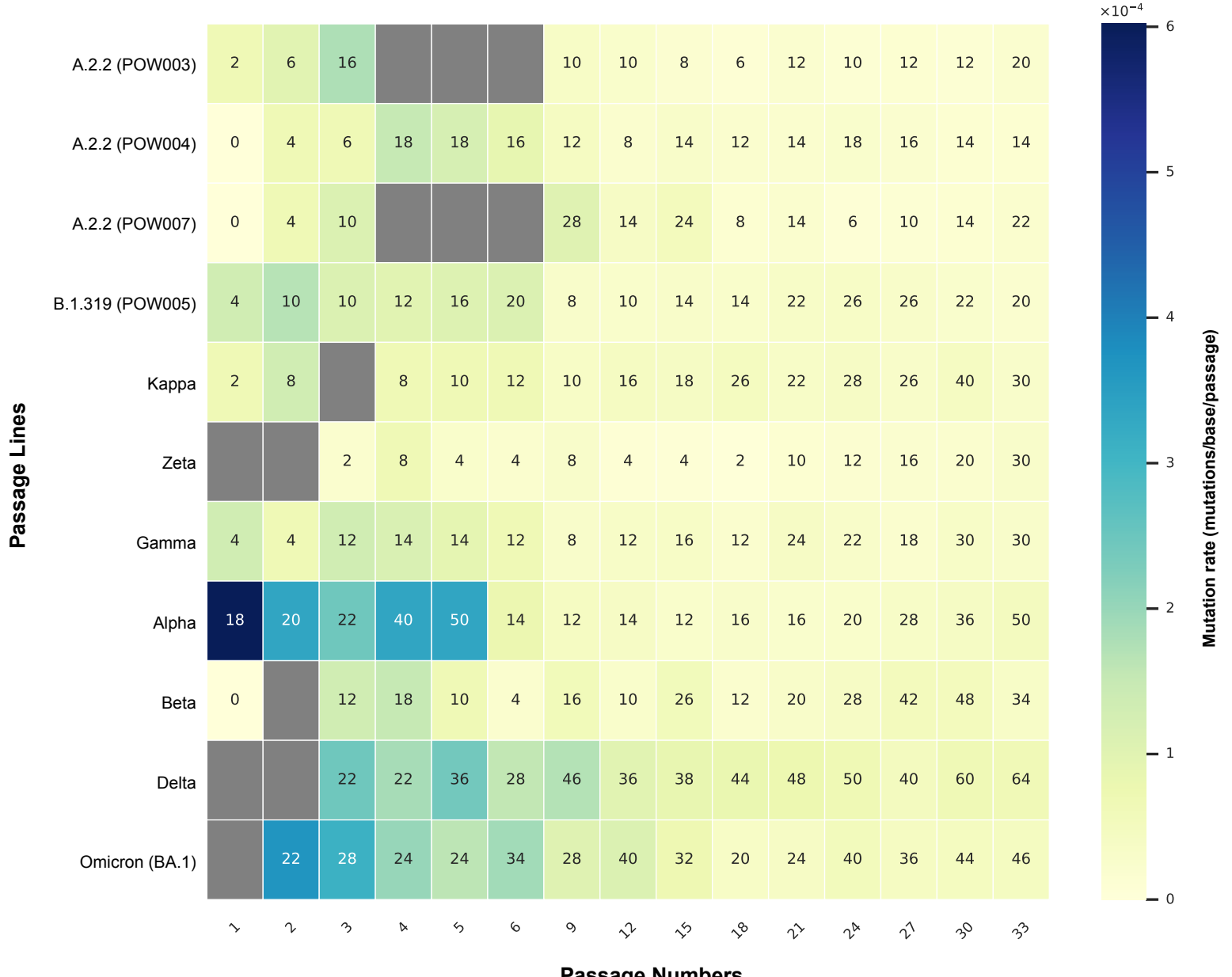
Passage Lines
A.2.2 (POW003) 2 6 16 10 10 8 6 12 10 12 12 20
A.2.2 (POW004) 0 4 6 18 18 16 12 8 14 12 14 18 16 14 14
A.2.2 (POW007) 0 4 10 28 14 24 8 14 6 10 14 22
B.1.319 (POW005) 4 10 10 12 16 20 8 10 14 14 22 26 26 22 20
Kappa 2 8 8 10 12 10 16 18 26 22 28 26 40 30
Zeta 2 8 4 4 8 4 4 2 10 12 16 20 30
Gamma 4 4 12 14 14 12 8 12 16 12 24 22 18 30 30
Alpha 18 20 22 40 50 14 12 14 12 16 16 20 28 36 50
Beta 0 12 18 10 4 16 10 26 12 20 28 42 48 34
Delta 22 22 36 28 46 36 38 44 48 50 40 60 64
Omicron (BA.1) 22 28 24 24 34 28 40 32 20 24 40 36 44 46
1 2 3 4 5 6 9 12 15 18 21 24 27 30 33
Passage Numbers
×10⁻⁴
0 1 2 3 4 5 6
Mutation rate (mutations/base/passage)

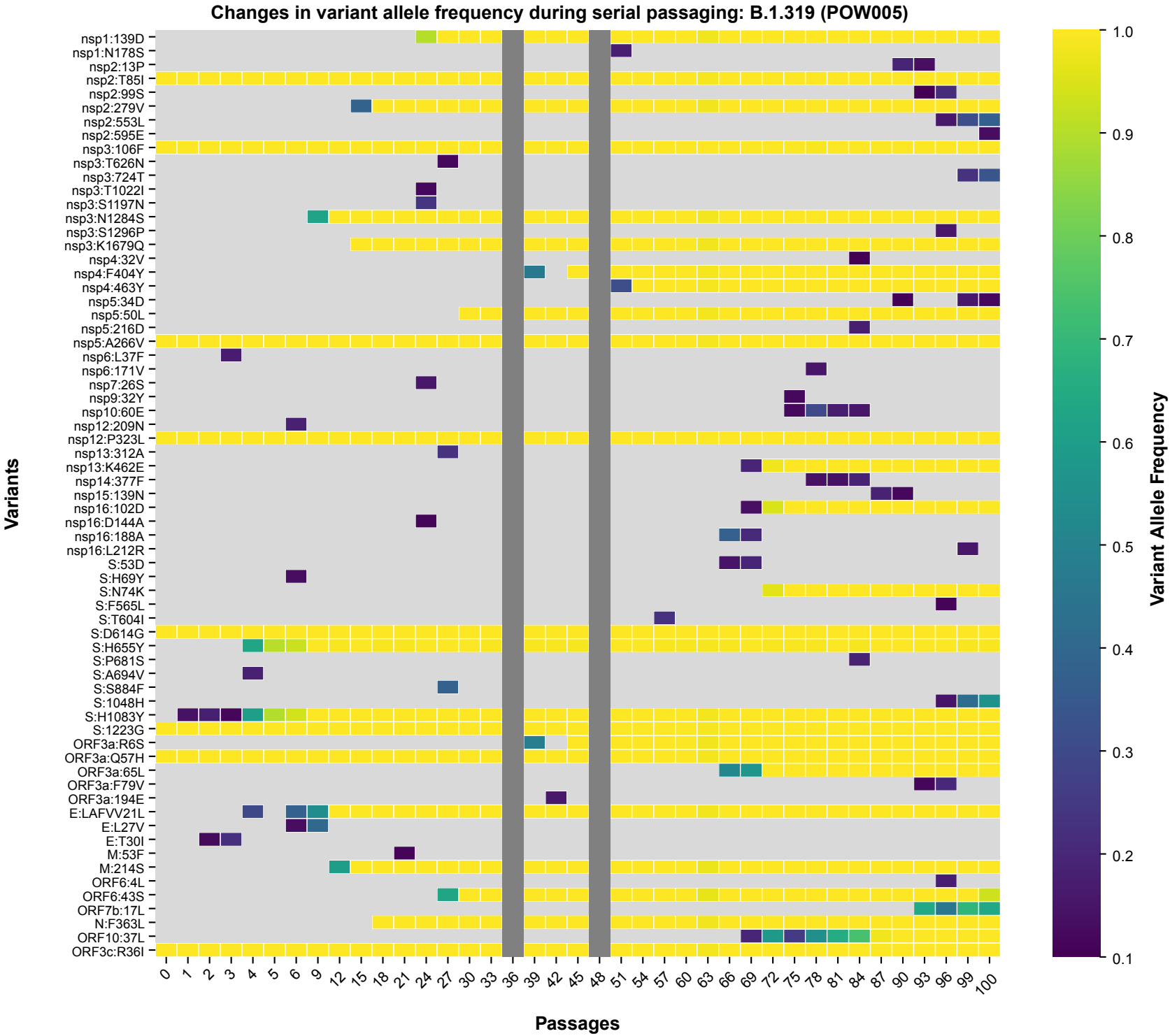
Changes in variant allele frequency during serial passaging: B.1.319 (POW005)
Variants
nsp1:139D
nsp1:N178S
nsp2:13P
nsp2:T85I
nsp2:99S
nsp2:279V
nsp2:553L
nsp2:595E
nsp3:106F
nsp3:T626N
nsp3:724T
nsp3:T1022I
nsp3:S1197N
nsp3:N1284S
nsp3:S1296P
nsp3:K1679Q
nsp4:32V
nsp4:F404Y
nsp4:463Y
nsp5:34D
nsp5:50L
nsp5:216D
nsp5:A266V
nsp6:L37F
nsp6:171V
nsp7:26S
nsp9:32Y
nsp10:60E
nsp12:209N
nsp12:P323L
nsp13:312A
nsp13:K462E
nsp14:377F
nsp15:139N
nsp16:102D
nsp16:D144A
nsp16:188A
nsp16:L212R
S:53D
S:H69Y
S:N74K
S:F565L
S:T604I
S:D614G
S:H655Y
S:P681S
S:A694V
S:S884F
S:1048H
S:H1083Y
S:1223G
ORF3a:R6S
ORF3a:Q57H
ORF3a:65L
ORF3a:F79V
ORF3a:194E
E:LAFVV21L
E:L27V
E:T30I
M:53F
M:214S
ORF6:4L
ORF6:43S
ORF7b:17L
N:F363L
ORF10:37L
ORF3c:R36I
0 1 2 3 4 5 6 9 12 15 18 21 24 27 30 33 36 39 42 45 48 51 54 57 60 63 66 69 72 75 78 81 84 87 90 93 96 99 100
Passages
Variant Allele Frequency
1.0
0.9
0.8
0.7
0.6
0.5
0.4
0.3
0.2
0.1

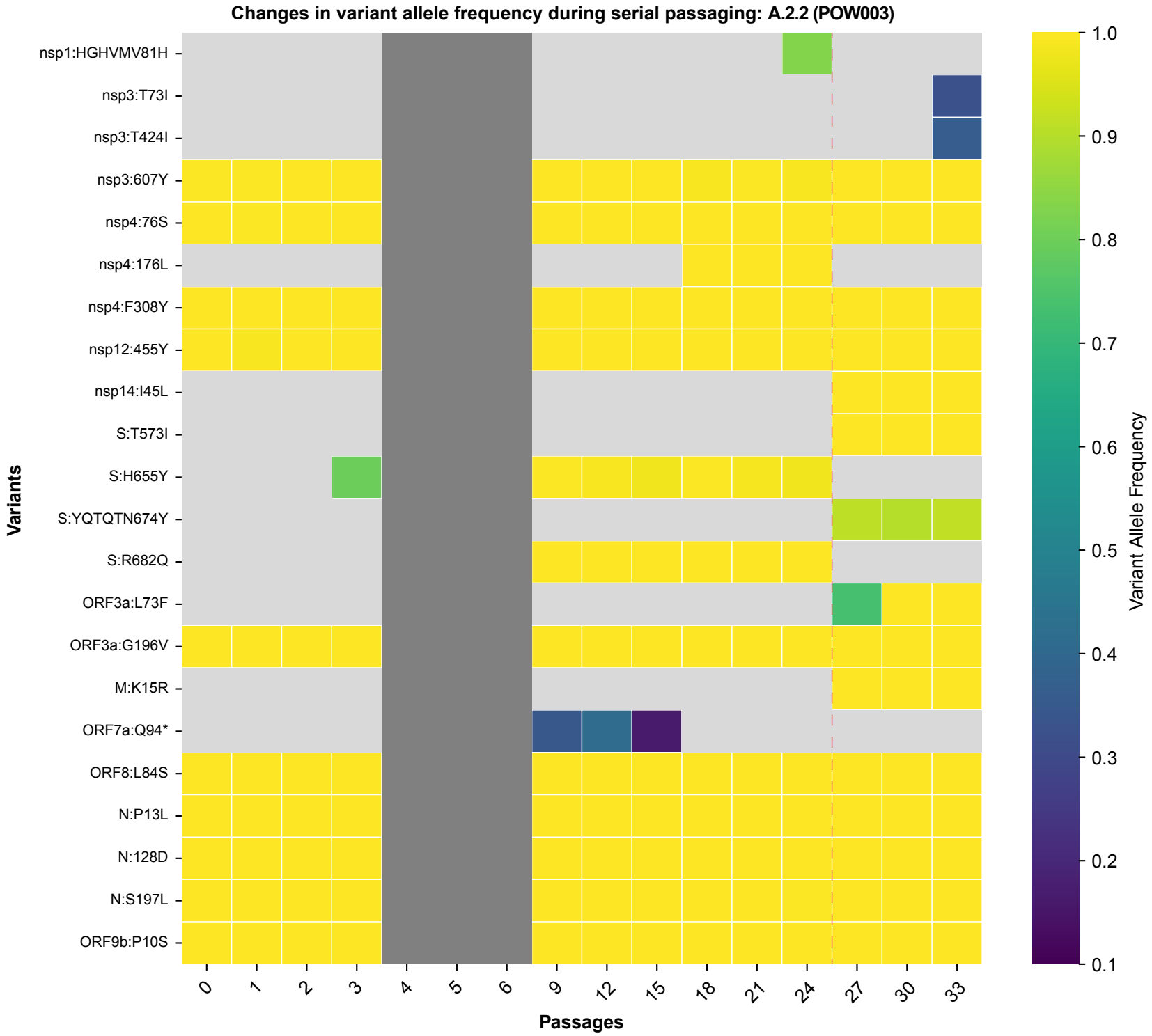
Changes in variant allele frequency during serial passaging: A.2.2 (POW003)
Variants
nsp1:HGHVMV81H
nsp3:T73I
nsp3:T424I
nsp3:607Y
nsp4:76S
nsp4:176L
nsp4:F308Y
nsp12:455Y
nsp14:I45L
S:T573I
S:H655Y
S:YQTQTN674Y
S:R682Q
ORF3a:L73F
ORF3a:G196V
M:K15R
ORF7a:Q94*
ORF8:L84S
N:P13L
N:128D
N:S197L
ORF9b:P10S
0
1
2
3
4
5
6
9
12
15
18
21
24
27
30
33
Passages
Variant Allele Frequency
1.0
0.9
0.8
0.7
0.6
0.5
0.4
0.3
0.2
0.1